Eur Biophys J (2012) 41:571–578
DOI 10.1007/s00249-012-0811-y

BIOPHYSICS LETTER

EBSA
Biophysics in Europe

Blood oxygenation using microbubble suspensions

Noriaki Matsuki · Shingo Ichiba · Takuji Ishikawa · Osamu Nagano · Motohiro Takeda · Yoshihito Ujike · Takami Yamaguchi

Received: 24 November 2011 / Revised: 12 March 2012 / Accepted: 22 March 2012 / Published online: 3 April 2012

Abstract Microbubbles have been used in a variety of fields and have unique properties, for example shrinking collapse, long lifetime, efficient gas solubility, a negatively charged surface, and the ability to produce free radicals. In medicine, microbubbles have been used mainly as diagnostic aids to scan various organs of the body, and they have recently been investigated for use in drug and gene delivery. However, there have been no reports of blood oxygenation by use of oxygen microbubble fluids without shell reagents. In this study, we demonstrated that nano or microbubbles can achieve oxygen supersaturation of fluids, and may be sufficiently small and safe for infusion into blood vessels. Although Po_2 increases in fluids resulting from use of microbubbles were inhibited by polar solvents, normal saline solution (NSS) was little affected. Thus, NSS is suitable for production of oxygen-rich fluid. In addition, oxygen microbubble NSS effectively improved hypoxic conditions in blood. Thus, use of oxygen microbubble (nanobubble) fluids is a potentially effective novel method for oxygenation of hypoxic tissues, for infection control, and for anticancer treatment.

Keywords Oxygenation · Microbubble · Nanobubble · Microbubble fluid · Fluid oxygenation

N. Matsuki (✉)
Department of Biomedical Engineering, Graduate School of Engineering, Okayama University of Science, 1-1, Ridai-cho, Kita-ku, Okayama 700-0005, Japan
e-mail: nmatsuki@bme.ous.ac.jp

S. Ichiba · O. Nagano · Y. Ujike
Department of Emergency and Critical Care Medicine, Okayama University School of Medicine and Hospital, 2-5-1, Shikata-cho, Kita-ku, Okayama 700-8558, Japan

T. Ishikawa · T. Yamaguchi
Department of Bioengineering and Robotics, Graduate School of Engineering, Tohoku University, 6-6-01, Aoba, Aramaki, Aoba-ku, Sendai 980-8579, Japan

M. Takeda · T. Yamaguchi
Department of Bioengineering, Graduate School of Biomedical Engineering, Tohoku University, 6-6-01, Aoba, Aramaki, Aoba-ku, Sendai 980-8579, Japan

Introduction

Microbubbles are miniature gas bubbles, <50 μm in diameter, in liquids, which mostly contain oxygen or air (Kurup and Naik 2010; Qin et al. 2009). Microbubbles have been used in a variety of ways: in soil fermentation and hydroponic plant growth, in aquaculture, for environmental improvement of water and sewage treatment, and in engineering production. Microbubbles have several unique properties (Takahashi et al. 2003, 2005, 2007). They remain relatively stable in water for a long time (they have a long lifetime), or rise very slowly, gradual shrink, and finally collapse (i.e., shrinking collapse), whereas macrobubbles increase in size, rise rapidly, and burst at the water surface. The internal pressure of microbubbles is also much higher than that of the local environment, which accelerates dissolution of the gas into the liquid (i.e., efficient gas solubility). They also have a negatively charged surface, and thus will not merge to form larger bubbles, and the ability to produce free radicals, for example –OH.

The most beneficial property of microbubbles is the highly efficient gas solubility. The mechanism of supersaturation of oxygen gas in water is expressed by the Young–Laplace equation (Takahashi et al. 2007):

$$P = P_l + 2\sigma/r$$

where P is the gas pressure, P_l is the liquid pressure, σ is the surface tension of the liquid, and r is the bubble radius. Inertial gas pressure is higher for smaller bubbles, so the inertial pressure of shrinking microbubbles increases with decreasing size. According to Henry's law, the amount of dissolved gas around the shrinking bubble increases with increasing gas pressure. DP is defined as the inertial increase in gas pressure relative to environmental pressure:

$$DP = 2\sigma/r = 4\sigma/2r = 4\sigma/D$$

where D is the bubble diameter.

For microbubbles 10 μm in diameter, the surface tension of water is 72.8 mN/m at 20 °C and DP is approximately 0.3 atm. However, when the microbubble diameter becomes 1 μm, DP increases tenfold (to approx. 3 atm).

Hypoxia, a condition of inadequate oxygen supply to tissues or the body, can lead to severe tissue damage and can be life threatening. Tissue hypoxia can develop if there is a decrease in cardiac output (ischemic hypoxia), hemoglobin concentration (anemic hypoxia), or oxygen saturation (hypoxic hypoxia), or an increase in the metabolic demands of the body (Abdelsalam and Cheifetz 2010). Hypoxia also induces physiological, cellular, and biochemical responses, which can effect pharmacological metabolism (Taylor and Moncada 2010; Ward et al. 2011, Donovan et al. 2010). Thus hypoxia is the most crucial issue in the treatment of a variety of diseases.

In medicine, microbubbles have been used as diagnostic aids to scan various organs of the body (Badea et al. 2009; Dijkmans et al. 2004; Lapotko 2011) and they have been studied for use in drug delivery and gene delivery (Dijkmans et al. 2004; Lapotko et al. 2011; Juffermans et al. 2004). There have recently been reports on use of microbubbles as local drug-delivery systems, using ultrasound with special shell reagents (Xu et al. 2011; Ferrara et al. 2009). However, biocompatibility of the shell reagents and ultrasound damage to the body are major problems that remain to be solved, as also is microbubble stability (Juffermans et al. 2006). Reports have also focused on special shell reagents for packing oxygen gas into microbubbles to extend the duration of oxygen delivery for injections (Cavalli et al. 2009; Swanson et al. 2010). In clinical applications of oxygen delivery to hypoxic patients, intravenous drip infusion is preferable because a large amount can be administered at once or over a long time.

Commonly used methods for generating microbubble suspensions are mechanical agitation, sonication, and pressurized gas–liquid mixing (microchannel emulsification); these usually result in the formation of microbubbles with wide size distributions. Gas–liquid mixing systems are preferable for generation of large amounts of microbubble suspensions at once, and bubble sizes are smaller. However, blood cannot be used directly in the machine because of blood cell destruction.

Therefore, methods for preparing fluids containing oxygen microbubbles (oxygen microbubble fluids) from conventional clinical fluids by use of gas–liquid mixing systems will be useful. There are no reports of blood oxygenation by use of oxygen microbubble fluids without shell reagents. This study was performed to determine:

- whether microbubbles could be used to efficiently increase the level of dissolved oxygen in liquids;
- how dissolved molecules such as electrolytes (e.g., NaCl) or glucose affect oxygenation of liquids; and
- whether oxygen microbubble fluid can improve oxygenation of hypoxic blood.

We found that normal saline solution (NSS) containing oxygen microbubbles (OMNSS) improves hypoxic conditions in blood.

Methods

Liquid solutions and blood samples

Sodium chloride and glucose (Wako Pure Chemical Industries, Osaka, Japan) were dissolved in ultrapure water as 1–10 % and 5–20 % solutions, respectively.

Approximately 100 ml blood was collected in a blood bag for autologous blood transfusion (Terumo CPDA blood bag, 200 ml; Terumo, Tokyo, Japan), from the ear vein of a healthy swine under general anesthesia, and stored in a refrigerator at 4 °C for 4 weeks. Each blood sample was taken from the blood bag by use of a disposable syringe (Terumo syringe, 2.5 ml; Terumo, Tokyo, Japan) to avoid contamination with air.

NSS (Otsuka Pharmaceutical, Tokyo, Japan) containing oxygen microbubbles was mixed with blood in dilution ratios of 10, 20, 30, 50 %. The samples were then gently shaken for 3 min before use in experiments.

These experiments were approved as animal experiment "no. 22-5" by the Ethics Review Committee for Animal Experimentation of Okayama University of Science.

Generation of microbubbles

Fine microbubbles of oxygen gas were generated by use of a micro-nanobubble aerator (AS-MA II; Asupu, Shizuoka, Japan), with hydrodynamic function, for 15 min, during which time oxygen gas was supplied at 1 l/min (Fig. 1). In the apparatus, water or another liquid (150 ml), introduced by a pump, spirals up along a wall and down to an outlet along the center of the apparatus. The centrifugal force

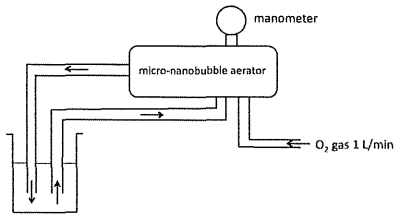

Fig. 1 Experimental setup. Relatively fine microbubbles of oxygen gas were generated by use of a micro-nanobubble aerator, at a peak pressure of 1–1.5 MPa, through which water or another liquid (150 ml) was circulating, for 15 min, and to which oxygen gas was supplied at 1 l/min. Fine microbubbles of oxygen gas were generated after brief sonication

caused by the circulation automatically introduces oxygen gas from the gas inlet and a vortex of oxygen gas is formed along the central axis. The body of the oxygen gas is separated into fine bubbles at the outlet of the apparatus by the strong shearing force of the dispersed water/liquid and circulation power. After generating water/liquid with oxygen gas microbubbles, the fluid was exposed to an ultrasonic bath (AUC-1L; As One, Osaka, Japan) for a few seconds to eliminate relatively large microbubbles.

For comparison purposes, macrobubbles were generated by use of an aquarium air stone (Round Air Stone S-2S; Daiko, Nagoya, Japan), to which oxygen gas was supplied at 1 l/min.

Morphological analysis of oxygen microbubbles generated in liquid

After brief sonication each 10 μm of the ultrapure water containing oxygen microbubbles was immediately mounted on a dual chamber slide (TC10™ System Sample Slides; Bio-Rad, Hercules, CA, USA). The oxygen microbubbles were then captured by microscopy (BZ-8100; Keyence, Tokyo, Japan), morphologically analyzed, and the bubble sizes measured.

Evaluation of dissolved oxygen in liquid or blood samples

After application of brief sonication, each fluid containing oxygen microbubbles was left for 30 s. The dissolved oxygen partial pressure (Po_2) in each liquid and blood sample mixed gently with NSS containing oxygen microbubbles for 3 min was then immediately measured, as an index of oxygenation, by use of a blood gas analyzer (ABL510; Radiometer, Copenhagen, Denmark). Each sample was taken by use of a disposable syringe to avoid contamination with air at room temperature (25 °C).

Statistical analysis

Results from the experiments are shown as the mean ± standard error of the mean (SEM). Statistical analysis was performed using StatMate III software (ATMS, Tokyo, Japan). Means were compared by use of unpaired *t* tests, or by analysis of variance (ANOVA) and Tukey's post-hoc test. In all analyses, $P < 0.05$ was taken as indicative of statistical significance.

Results

Generation of microbubbles

To confirm the generation of fine microbubbles by the micro-nanobubble aerator, ultrapure water containing fine oxygen microbubbles was morphologically analyzed by microscopy.

Figure 2a shows the distribution of oxygen microbubbles in ultrapure water after circulation through the micro-nanobubble aerator—96.2 % of the generated oxygen bubbles were less than 50 μm in diameter (microbubble). Most (35.7 %) microbubbles were 20–30 μm in diameter, and a significant amount (26.2 %) of relatively fine microbubbles less than 20 μm in diameter was also present.

Figure 2b shows the fine oxygen microbubbles generated after brief sonication. Bubbles were less than 10 μm in diameter and inhomogeneous (ranging from <1 to 6 μm in diameter). Some fine microbubbles were seen to shrink and collapse during morphological analysis.

Evaluation of dissolved oxygen in liquids containing macrobubbles and microbubbles

To examine the potency of microbubbles for dissolving oxygen gas in liquid, the Po_2 in ultrapure water was compared between macrobubbles ($f > 1$ mm) and microbubbles by blood gas analysis. Figure 3 shows the Po_2 values in ultrapure water. Means were compared by ANOVA and Tukey's post-hoc test. On average, oxygen gas was dissolved with Po_2 of 170 ± 5.6 mmHg (mean ± SEM) in the control ($P < 0.01$ vs. macro and microbubbles), 776.8 ± 19.3 mmHg in ultrapure water exposed to oxygen macrobubbles ($P < 0.01$ vs. control and microbubbles), and 1,003.2 ± 25.5 mmHg in ultrapure water containing oxygen microbubbles ($P < 0.01$ vs. control and macrobubbles). These results suggest that oxygen microbubbles could significantly increase the Po_2 values in ultrapure water compared with macrobubbles.

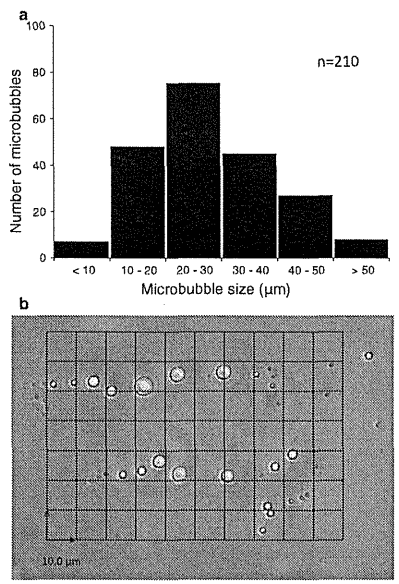

Fig. 2 Morphological analysis of generated oxygen microbubbles. a The distribution of the microbubbles generated by the micro-nanobubble aerator. b Microbubbles were inhomogeneous in size. After brief sonication, relatively large microbubbles disappeared and fine microbubbles remained. The bubbles were <6 μm in diameter and nanobubbles were also present

Effects of solvents on the Po_2 increase by microbubbles

To examine the effect of solvent on the Po_2 increase after microbubble treatment, the Po_2 in ultrapure water containing a 1, 5, or 10 % NaCl, an electrolyte, or a 5, 10, or 20 % glucose, were measured by blood gas analysis. Means were compared by ANOVA and Tukey's post-hoc test.

Figure 4a shows the effects of NaCl on Po_2 increase by use of oxygen microbubbles. On average, Po_2 values were 1,003.2 ± 25.5 mmHg in the control ($P < 0.01$ vs. 5 % and 10 % NaCl solution), 985.6 ± 27.1 mmHg in 1 % NaCl solution ($P < 0.01$ vs. 5 % and 10 % NaCl solution), 829.5 ± 18.6 mmHg in 5 % NaCl solution ($P < 0.01$ vs. control and 1 % NaCl solution), and 745.8 ± 11.4 mmHg in 10 % NaCl solution ($P < 0.01$ vs. control and 1 % NaCl solution). These results suggested that the oxygenation by microbubbles decreased with increasing concentration of the NaCl solution. Above, less than 1 % NaCl solution was enough to increase the Po_2 in the liquid by use of oxygen microbubbles compared with untreated ultrapure water.

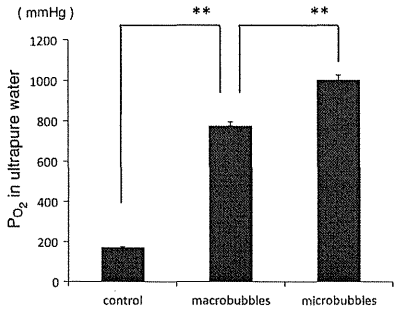

Fig. 3 Comparison of Po_2 increase in ultrapure water between oxygen macrobubbles and oxygen microbubbles. Oxygen macrobubbles were generated in ultrapure water (150 ml) by use of porous ceramic with 1 l/min oxygen gas supply for 15 min. Oxygen microbubbles were generated by use of a micro-nanobubble aerator. The Po_2 in ultrapure water was determined by blood gas analysis. Results are shown as mean ± standard error of the mean from five separate experiments, each performed in duplicate. $^{**}P < 0.01$

Figure 4b shows the effects of glucose on the Po_2 increase by use of oxygen microbubbles. On average, Po_2 values were 1,003.2 ± 25.5 mmHg in the control ($P < 0.05$ vs. 5 % glucose solution, $P < 0.01$ vs. 10 and 20 % glucose solution), 866.3 ± 38.6 mmHg in 5 % glucose solution ($P < 0.05$ vs. control), 828.3 ± 17.8 mmHg in 10 % glucose solution ($P < 0.01$ vs. control), and 763.8 ± 29.8 mmHg in 20 % glucose solution ($P < 0.01$ vs. control). The results suggested that oxygenation by microbubbles decreased with increasing concentration of glucose. Even 5 % glucose solution significantly inhibited the Po_2 increase by oxygen microbubbles.

Blood oxygenation by use of oxygen microbubble fluid

To examine the potency of blood oxygenation by fluid containing oxygen microbubbles, OMNSS was mixed with swine venous blood in different ratios. After mixing for 3 min at dilution ratios of 10–50 %, the Po_2 in blood samples was measured by blood gas analysis.

Figure 5a shows Po_2 values in blood diluted with 10, 20, 30, or 50 % OMNSS or NSS. Means were compared by use of unpaired *t*-tests. The average Po_2 in control blood (without dilution) was 64.6 ± 1.3 mmHg. Average Po_2 values were 81.9 ± 3.3 mmHg and 72.4 ± 1.5 mmHg in blood diluted with 10 % OMNSS/NSS ($P < 0.05$), 89.5 ± 4.2 mmHg and 78.9 ± 2.5 mmHg in blood diluted

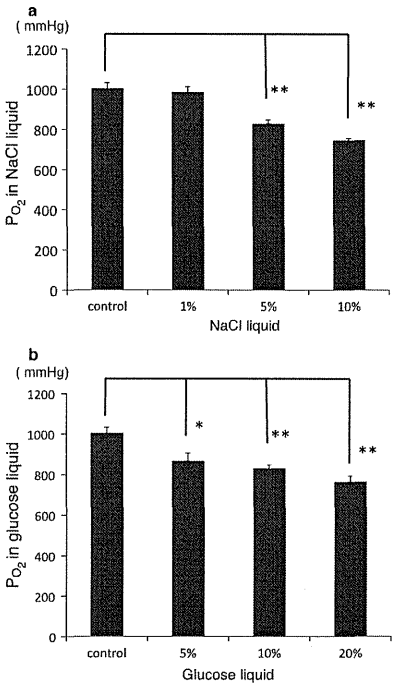

Fig. 4 Effects of solutes on the Po_2 increase in fluid resulting from use of oxygen microbubbles. a NaCl. b Glucose. Results are mean ± standard error of the mean from five separate experiments, each performed in duplicate. *$P < 0.05$; **$P < 0.01$

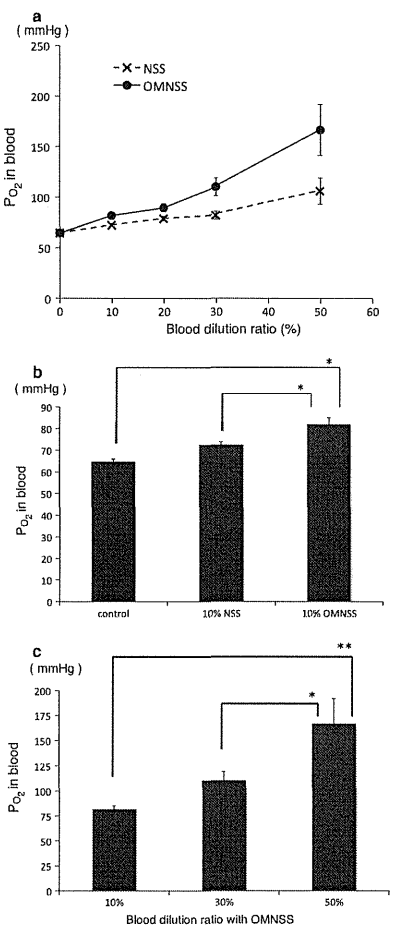

Fig. 5 Po_2 increases in blood by use of oxygen microbubble NSS (OMNSS). Swine venous blood was diluted with OMNSS at 10, 20, 30, or 50 %, and mixed gently for 3 min. The Po_2 in blood was determined by blood gas analysis. a Comparison of Po_2 increases in blood between NSS and OMNSS. b Comparison of Po_2 increases in blood at 10 % dilution with NSS or OMNSS. c Po_2 increases in blood at each dilution ratio with OMNSS. Results are shown as mean ± standard error of the mean from five separate experiments, each performed in duplicate. *$P < 0.05$; **$P < 0.01$

with 20 % OMNSS/NSS ($P < 0.05$), 110.4 ± 8.9 mmHg and 82.1 ± 4.1 mmHg in blood diluted with 30 % OMNSS/NSS ($P < 0.05$), and 166.6 ± 25.3 mmHg and 106.0 ± 13.1 mmHg in blood diluted with 50 % OMNSS/NSS ($P < 0.05$), respectively. These results suggest that OMNSS results in a significantly greater Po_2 increase in blood than NSS, and the difference in Po_2 value between OMNSS and NSS becomes greater with increasing dilution ratio in the blood.

Figure 5b shows Po_2 values at 10 % dilution with NSS with and without oxygen microbubbles in blood. Means were compared by ANOVA and Tukey's post-hoc test. On average, the Po_2 values were 64.6 ± 1.4 mmHg in control venous blood ($P < 0.05$ vs. 10 % OMNSS), 72.4 ± 1.5 mmHg in blood diluted 10 % with NSS ($P < 0.05$ vs. 10 % OMNSS), and 81.9 ± 3.3 mmHg in blood diluted 10 % with OMNSS ($P < 0.05$ vs. control and 10 % diluted blood with NSS). The results suggested that OMNSS significantly improved the Po_2 in hypoxic blood.

Figure 5c shows Po_2 values in blood diluted with 10, 30, or 50 % OMNSS. Means were compared by ANOVA and Tukey's post-hoc test. The average Po_2 values were 81.9 ± 3.3 mmHg in blood diluted with 10 % OMNSS ($P < 0.01$ vs. 50 %), 110.4 ± 8.9 mmHg in blood diluted with 30 % OMNSS ($P < 0.05$ vs. 50 %), and 166.6 ± 25.3 mmHg in blood diluted with 50 % OMNSS ($P < 0.01$ vs. 10 %, $P < 0.05$ vs. 30 %). These results suggested that Po_2 in hypoxic blood was significantly increased by increasing the mixing volume of OMNSS. In addition, blood diluted with 50 % OMNSS was significantly more oxygenated than 10 % diluted blood ($P < 0.05$).

Discussion

Microbubbles are gas bubbles <50 μm diameter in liquids; they have a variety of unique properties (Kurup and Naik 2010; Qin et al. 2009). In particular, their efficient and high oxygen gas solubility is beneficial for oxygenation of hypoxic tissues (Bitterman 2009; Abdelsalam and Cheifetz 2010; Raoof et al. 2010; Guo and DiPietro 2010).

In our experiments, most of the oxygen microbubbles generated after application of brief sonication were <10 μm in diameter (Fig. 2b), and were categorized as fine microbubbles (Takahashi et al. 2003, 2005, 2007). These fine microbubbles were thought to be captured as the result of the gradual shrinking of microbubbles that finally collapse. Fine oxygen microbubbles are expected to have a variety of useful properties in medicine (Barbosa et al. 2009; Betit 2009; Kulikovsky et al. 2009). Microbubbles <10 μm in diameter are thought to be clinically safe; the filter pore sizes for cardiopulmonary bypass machines are usually in the range 28–40 μm, and oxygen microbubbles 10 μm in diameter are therefore negligibly small (Barak and Katz 2005).

The most beneficial property of microbubbles is the highly efficient gas solubility, which is expressed as Po_2 increases in liquids including blood. The Po_2 values in water containing oxygen microbubbles were significantly higher than the theoretical Po_2 value (760 mmHg). According to the Young–Laplace equation, the shrinking oxygen microbubble increases the inertial pressure and oxygen gas dissolves to a much greater extent water by Henry's law. The smaller the bubble size, the higher the Po_2 value in water. In our experiments, Po_2 values in water were approximately 30 % greater than full oxygen saturation (Fig. 3). Nanobubbles must increase the Po_2 value in water to a much greater extent than microbubbles.

Next, we examined how solutes in the fluid, for example NaCl and glucose, which are commonly used in daily clinical practice, affect the increase in Po_2 by microbubbles. NaCl and glucose both inhibited the Po_2 increase by microbubbles, in accordance with their concentration (Fig. 4a). As oxygen gas has low polarity and tends to dissolve in low-polarity liquids, our results indicating that Po_2 in water was reduced by NaCl or glucose, which are polar in solution, are credible. However, NSS used in daily clinical practice is of very low concentration (only 0.9 %) and had little effect on the Po_2 values compared with the control. Therefore, NSS containing microbubbles can be a clinically useful fluid for tissue oxygenation. The Po_2 values in 5 % glucose solution were significantly (~15 %) reduced compared with the control. Twenty percent glucose solution, which is used in intravenous hyperalimentation, had almost the same Po_2 as the theoretical maximum Po_2 value in water (Fig. 4b). Thus, fluids containing glucose are not suitable for tissue oxygenation using this method.

OMNSS increased the Po_2 values in blood in accordance with the mixing volume (ratio) (Fig. 5a). At 10 % dilution in blood, OMNSS resulted in significantly higher Po_2 than NSS (Fig. 5b). The oxygen volume in blood is expressed as follows (Scholz et al. 2010):

$$\text{Total } Co_2 = (a \cdot Po_2 + b \cdot Hb \cdot \text{Sat}) \cdot V$$

where a is the solubility coefficient of oxygen in blood (0.003 ml/l mmHg), b is the oxygen-carrying capacity of hemoglobin (1.34 ml/gHb), Hb is the concentration of hemoglobin in blood (15 g/dl), V is blood volume (5 l), and Sat is the saturation of hemoglobin.

In addition, Sat in blood under conditions of pH 7.4 at 37 °C is expressed as follows (Dash and Bassingthwaighte 2010):

$$Sat = Ko_2 \cdot Po_2^n / (1 + Ko_2 \cdot Po_2^n) = (Po_2/P_{50})^n \{1 + (Po_2/P_{50})^n\}$$

where Ko_2 is the Hill coefficient and n is the Hill exponent ($n = 2.7$). They are related by $Ko_2 = (P_{50})^{-n}$ where P_{50} is the level of Po_2 at which Hb is 50 % saturated by O_2 ($P_{50} = 26.6$ mmHg) (Goutelle et al. 2008).

In this study, the mean Po_2 of the control blood (64.6 mmHg) was improved from 81.6 to 166.6 mmHg by dilution with OMNSS. Given these data at 37 °C, the saturation value of hemoglobin was calculated to be 91.3 % at $Po_2 = 64.6$ mmHg, 95.2 % at $Po_2 = 81.6$ mmHg, and 99.3 % at $Po_2 = 166.6$ mmHg. The total Co_2 was calculated as 927 ml for control blood, 970.8 ml for blood diluted with 10 % OMNSS, and 1004.3 for blood diluted with 50 % OMNSS. The value of total Co_2 for blood diluted with 10 % OMNSS was 43.8 ml higher than that of the control blood; this oxygen excess corresponds to

87.6 % of the oxygen consumption of the brain per minute in adults. In addition, the value of total Co_2 in blood diluted with 50 % OMNSS was 121 ml higher than that of the control blood; this oxygen excess corresponds to 48.4 % of the oxygen consumption of the whole body per minute in adults. Therefore, the oxygen microbubble fluid described here can be locally injected into hypoxic tissues but is not sufficient for general infusion. For general infusion, it will be necessary to achieve an approximately tenfold higher density of oxygen microbubbles. This will require more innovative methods for production of finer microbubbles (nanobubbles) or shell reagents for bubbles.

In summary, finer micro-nanobubbles can be used to achieve oxygen supersaturation in fluids, and may be small and safe enough for infusion into blood vessels. Although increases in Po_2 in fluids by use of oxygen microbubbles were inhibited by polar solvents, NSS had little effect. Thus, NSS will be suitable for production of oxygen-rich fluid. In addition, OMNSS effectively improved hypoxic conditions in blood. Use of oxygen micro/nanobubble fluids is an effective novel method for oxygenation of hypoxic tissues caused by ischemia and general hypoxia, for infection control caused by anaerobic bacteria, and for anticancer treatment. However, it has been suggested that microbubbles also cause tissue damage and that oxygen itself can be toxic (Barak and Katz 2005; Dennery 2010; Wang et al. 2010; Allen et al. 2009). Further studies of fine micro/nanobubbles are required to increase the Po_2 under hypoxic conditions and to assess the effects on tissues and the whole body.

Acknowledgments This study was supported by Grants-in-Aid for Scientific Research (C) from the Japan Society for the Promotion of Science (JSPS; no. 21500402).

References

Abdelsalam M, Cheifetz IM (2010) Goal-directed therapy for severely hypoxic patients with acute respiratory distress syndrome: permissive hypoxemia. Respir Care 55(11):1483–1490

Allen BW, Demchenko IT, Piantadosi CA (2009) Two faces of nitric oxide: implications for cellular mechanisms of oxygen toxicity. J Appl Physiol 106(2):662–667

Badea R, Seicean A, Diaconu B, Stan-Iuga R, Sparchez Z, Tantau M, Socaciu M (2009) Contrast-enhanced ultrasound of the pancreas: a method beyond its potential or a new diagnostic standard? J Gastrointestin Liver Dis 18(2):237–242

Barak M, Katz Y (2005) Microbubbles: pathophysiology and clinical implications. Chest 128(4):2918–2932

Barbosa FT, Juca MJ, Castro AA, Duarte JL, Barbosa LT (2009) Artificial oxygen carriers as a possible alternative to red cells in clinical practice. Sao Paulo Med J 127(2):97–100

Betit P (2009) Extracorporeal membrane oxygenation: Quo Vadis? Respir Care 54(7):948–957

Bitterman H (2009) Bench-to-bedside review: oxygen as a drug. Crit Care 13(1):205

Cavalli R, Bisazza A, Giustetto P, Civra A, Lembo D, Trotta G, Guiot C, Trotta M (2009) Preparation and characterization of dextran nanobubbles for oxygen delivery. Int J Pharm 381(2):160–165

Dash RK, Bassingthwaighte JB (2010) Erratum to: blood HbO_2 and $HbCO_2$ dissociation curves at varied O_2, CO_2, pH, 2,3-DPG and temperature levels. Ann Biomed Eng 38(4):1683–1701

Dennery PA (2010) Oxygen administration in the care of neonates: a double-edged sword. Chin Med J 123(20):2938–2942

Dijkmans PA, Juffermans LJ, Musters RJ, van Wamel A, ten Cate FJ, van Gilst W, Visser CA, de Jong N, Kamp O (2004) Microbubbles and ultrasound: from diagnosis to therapy. Eur J Echocardiogr 5(4):245–256

Donovan L, Welford SM, Haaga J, LaManna J, Strohl KP (2010) Hypoxia: implications for pharmaceutical developments. Sleep Breath 14(4):291–298

Ferrara KW, Borden MA, Zhang H (2009) Lipid-shelled vehicles: engineering for ultrasound molecular imaging and drug delivery. Acc Chem Res 42(7):881–892

Goutelle S, Maurin M, Rougier F, Barbaut X, Bourguignon L, Ducher M, Maire P (2008) The Hill equation: a review of its capabilities in pharmacological modeling. Fundam Clin Pharmacol 22(6):633–648

Guo S, DiPietro LA (2010) Factors affecting wound healing. J Dent Res 89(3):219–229

Juffermans LJ, Dijkmans PA, Musters RJ, van Wamel A, Bouakaz A, ten Cate FJ, Deelman L, Visser CA, de Jong N, Kamp O (2004) Local drug and gene delivery through microbubbles and ultrasound: a safe and efficient alternative for viral vectors? Neth Heart J 12(9):394–399

Juffermans LJ, Dijkmans PA, Musters RJ, Visser CA, Kamp O (2006) Transient permeabilization of cell membranes by ultrasound-exposed microbubbles is related to formation of hydrogen peroxide. Am J Physiol Heart Circ Physiol 291(4):H1595–H1601

Kulikovsky M, Gil T, Mattanes I, Karmeli R, Har-Shai Y (2009) Hyperbaric oxygen therapy for non-healing wounds. Isr Med Assoc J 11(8):480–485

Kurup N, Naik P (2010) Microbubbles, A novel delivery system. J Pharmaceut Res Health Care 2(3):228–234

Lapotko D (2011) Plasmonic nanobubbles as tunable cellular probes for cancer theranostics. Cancers 3(1):802–840

Qin S, Caskey CF, Ferrara KW (2009) Ultrasound contrast microbubbles in imaging and therapy: physical principles and engineering. Phys Med Biol 54(6):R27–R57

Raoof S, Goulet K, Esan A, Hess DR, Sessler CN (2010) Severe hypoxemic respiratory failure: part2-nonventilatory strategies. Chest 137(6):1437–1448

Scholz AW, Eberle B, Heussel CP, David M, Schmittner MD, Quintel M, Schreiber LM, Weiler N (2010) Ventilation-perfusion ratio in Perflubron during partial liquid ventilation. Anesth Analg 110(6):1661–1668

Swanson EJ, Mohan V, Kheir J, Borden MA (2010) Phospholipid-stabilized microbubble foam for injectable oxygen delivery. Langmuir 26(20):15726–15729

Takahashi M (2005) The ζ potential of microbubbles in aqueous solutions, Electrical property of the gas-water interface. J Phys Chem B 109(46):21858–21864

Takahashi M, Kawamura T, Yamamoto Y, Ohnari H, Himuro S, Shakutsui H (2003) Effect of shrinking microbubble on gas hydrate formation. J Phys Chem B 107(10):2171–2173

Takahashi M, Chiba K, Li P (2007) Free-radical generation from collapsing microbubbles in the absence of a dynamic stimulus. J Phys Chem B 111(6):1343–1347

Taylor CT, Moncada S (2010) Nitric oxide, cytochrome C oxidase, and the cellular response to hypoxia. Arterioscler Thromb Vasc Biol 30(4):643–647

Wang C, Zhang X, Liu F, Paule MG, Slikker W Jr (2010) Anesthetic-induced oxidative stress and potential protection. Sci World J 10:1473–1482

Ward DS, Karan SB, Pandit JJ (2011) Hypoxia: developments in basic science, physiology and clinical studies. Anaesthesia 66(Suppl 2):19–26

Xu Q, Nakajima M, Liu Z, Shiina T (2011) Biosurfactants for microbubble preparation and application. Int J Mol Sci 12(1):462–475

Endocrine Journal 2013, 60 (2), 137-147

ORIGINAL

Characterization of contraction-induced IL-6 up-regulation using contractile C2C12 myotubes

Arta Farmawati[1)*], Yasuo Kitajima[1)], Taku Nedachi[2)], Masaaki Sato[3)], Makoto Kanzaki[3), 4)] and Ryoichi Nagatomi[1), 3)]

[1)] *Department of Medicine & Science in Sports & Exercise, Graduate School of Medicine, Tohoku University, Sendai 980-8575, Japan*
[2)] *Faculty of Life Sciences, Toyo University, Gunma 374-0193, Japan*
[3)] *Graduate School of Biomedical Engineering, Tohoku University, Sendai 980-8579, Japan*
[4)] *Core Research for Evolutional Science and Technology, Japan Science and Technology Agency (JST), Japan*

Abstract. Muscle contractile activity functions as a potent stimulus for acute interleukin (IL)-6 expression in working skeletal muscles. Recently, we established an "*in vitro* contraction model" using highly-developed contractile C2C12 myotubes by applying electric pulse stimulation (EPS). Herein, we characterize the effects of EPS-evoked contraction on IL-6 expression in contractile C2C12 myotubes. Both secretion and mRNA expression of IL-6 were significantly up-regulated by EPS in a frequency-dependent manner in contracting myotubes during a 24-h period, and the response was blunted by cyclosporine A, a calcineurin inhibitor. Longer time (~12h) was required for the induction of IL-6 after the initiation of EPS as compared to that of other contraction-inducible CXC chemokines such as CXCL1/KC, which were induced in less than 3 hours. Furthermore, these acute inducible CXC chemokines exhibited no autocrine effect on IL-6 expression. Importantly, contraction-dependent IL-6 up-regulation was markedly suppressed in the presence of high levels of glucose along with increased glycogen accumulations. Experimental manipulation of intracellular glycogen contents by modulating available glucose or pyruvate during a certain EPS period further established the suppressive effect of glycogen accumulations on contraction-induced IL-6 up-regulation, which appeared to be independent of calcineurin activity. We also document that EPS-evoked contractile activity improved insulin-responsiveness in terms of intracellular glycogen accumulations. Taken together, these data provide important insights into the regulation of IL-6 expression in response to contractile activity of muscle cells, which is difficult to examine using *in vivo* experimental techniques. Our present results thus expand the usefulness of our "*in vitro* contraction model".

Key words: Exercise, Myokine, IL-6, Glycogen, Insulin

IT HAS BECOME increasingly apparent that skeletal muscle functions as an endocrine organ that secretes a number of cytokines, including interleukin (IL)-1β, IL-6, IL-8, IL-10, and IL-15 and that physical activity induces some of these muscle-derived myokines, which are therefore referred to as "exercise factors" [1, 2]. IL-6 expression in muscle is well known to be up-regulated by physical activity, both at the mRNA and the protein level, which is indeed responsible for the increases in the levels of systemic IL-6 concentration after exercise in rodents and human subjects [3-6]. Importantly, IL-6 was shown to have positive effects on skeletal muscle glucose disposal [7, 8], and accumulating evidence demonstrated that some of the beneficial effects of exercise might be mediated by exercise factors including IL-6 [9]. Thus, understanding of the mechanistic details of IL-6 expression in skeletal muscles in response to their contractile activity is an important issue, with health implications especially for patients with type 2 diabetes.

A key issue in understanding the effect of contractile activity on IL-6 up-regulation is to clarify the intracellular signaling mechanisms by which cells can decipher and respond to a highly complex mechanical stimulus associated with acute energy fluctuations, which is apparently further influenced by environmental circumstances including blood flow and nutrient conditions as well as various humoral factors including autocrine/paracrine factors derived from working skeletal muscles. Indeed, several studies have demonstrated that glucose availability and/or muscle glycogen contents influenced the rate of IL-6 expression and the release from working skeletal muscle [10-12] and that exercise-induced IL-6 production is significantly augmented under low glycogen conditions in muscle [13, 14]. In addition, several lines of evidence indicated that levels of IL-6 expression in skeletal muscle was modulated by various cytokines including IL-6 itself [15, 16]. However, the precise molecular mechanism by which exercise regulates IL-6 expression under diverse nutritional circumstances is poorly understood, which is at least partially due to limitations stemming from the conventional *in vivo* exercise experiments that make it difficult to precisely control nutritional/humoral circumstances *in vivo*.

We recently succeeded in establishing an advanced *in vitro* muscle exercise model using highly developed C2C12 myotubes possessing electric pulse stimulation (EPS)-evoked vigorous contractile activity. Importantly, we have observed that these highly developed C2C12 myotubes displayed some important aspects of beneficial effects of exercise such as improved insulin sensitivity and fiber type switching after EPS-evoked contractile activity [17]. In addition, the contractile C2C12 myotubes appeared to have the ability to secrete various chemokines/cytokines including IL-6 and CXCL1/KC in response to EPS [17, 18], approximating those observed in working skeletal muscle *in vivo* [17]. In order to understand exercise-induced IL-6 up-regulation in working skeletal muscles, we took advantage of our *in vitro* exercise model and investigated the characteristics of IL-6 production from the C2C12 myotubes in response to EPS-evoked contractile activity in detail. In addition, we attempted to clarify possible influences of CXCL1/KC, a newly identified myokine, on the EPS-evoked IL-6 expression in contractile myotubes. The effects of ambient glucose levels on IL-6 expression were also investigated.

Materials and Methods

Materials

Cell culture equipment was purchased from BD Biosciences (San Jose, CA, USA). Dulbecco's Modified Eagle Medium (DMEM), penicillin/streptomycin and Trypsin-EDTA were purchased from Sigma Chemicals (St. Louis, MO, USA). Calf serum (CS) and fetal bovine serum (FBS) were purchased from BioWest (Nuaille, France). The Western blot detection kit (West super femto detection reagents) was purchased from Thermo Fisher Scientific Inc. (Rockford, IL, USA). Immobilon-P was purchased from Millipore Corp. (Bedford, MA, USA). Bovine serum albumin (BSA) was purchased from Wako (Osaka, Japan). The enzyme-linked Immunosorbent Assay (ELISA) kit for IL-6 was obtained from eBioscience (San Diego, CA, USA). Unless otherwise noted, all chemicals were of the purest grade available from Wako or Sigma Chemicals.

Cell culture

A mouse skeletal muscle cell line, C2C12 myoblast [19], was grown on 4-well plates (BD Biosciences) at a density of 0.5×10^5 cells/well in 5 mL of growth medium. Briefly, C2C12 myoblasts were culture in the growth medium, DMEM containing 25 mM glucose (high glucose; HG) supplemented with 10% FBS, 100 μg/mL penicillin, and 100 μg/mL streptomycin, at 37°C under a 5% CO_2 atmosphere for 3-4 days until ~80-90% confluence (day 0). Differentiation was then induced by switching the growth medium to DMEM supplemented with 2% CS, 1 nM insulin, 30 μg/mL penicillin, and 100 μg/mL streptomycin (differentiation medium) [20]. The differentiation medium was changed every 24 hours. The cells were then incubated in DMEM containing 5 mM (low glucose; LG) or 25 mM (HG) glucose under the indicated conditions.

Electrical pulse stimulation (EPS)

Five to six days after differentiation, the differentiated C2C12 myotubes in 4-well plates were placed in a chamber for EPS (C-Dish, IonOptix, Milton, MA). EPS was applied to the cells in the C-Dish using a C-Pace pulse generator (C-Pace 100, IonOptix, Milton MA). The stimulator was set to deliver a pulse with a 2-ms duration, 40 V/60 mm voltage and 0.1 or 1 Hz frequency [17]. The cells in the C-Dish were placed inside a humidified incubator at 37°C under 5% CO_2 atmosphere.

Submitted Aug. 23, 2012; Accepted Sep. 6, 2012 as EJ12-0316
Released online in J-STAGE as advance publication Sep. 30, 2012

Correspondence to: Makoto Kanzaki, Ph.D., Graduate School of Biomedical Engineering, Tohoku University, 6-6-11-901/2, Aoba, Aramaki, Aoba-ku, Sendai 980-8579, Japan.
E-mail: kanzaki@bmc.tohoku.ac.jp

*A.F., current address: Faculty of Medicine, Gadjah Mada University, Indonesia

ELISA for IL-6 concentration

Conditioned media were collected at the indicated time point and stored at -20°C until IL-6 analysis. The concentration of IL-6 secreted into the culture media was measured using the Mouse Interleukin-6 ELISA Ready-SET-Go! (eBioscience) according to the manufacturer's instructions (detection limit: 4 pg/mL). Three or four independent experiments were performed for each experimental condition.

Real-time PCR analysis of gene expression

Total RNA was prepared using the TRIzol reagent (Invitrogen) and quantitative real-time PCR analysis was performed using the Light Cycler instrument and SYBR Green detection kit (Roche Diagnostics, IN, USA). Primers for IL-6 (mouse IL-6 LightCycler™-Primer Set, GenBank Accession: NM_031168) were purchased from Nihon Gene Research Laboratories Inc. (Japan). Primers for β-actin as a control were: 5'-CGT TGA CAT CCG TAA AGA CCT C-3' and 5'-AGC CAC CGA TCC ACA CAG A-3'.

Western blot analysis

Cells were lysed with lysis buffer (30 mM Tris pH 7.4, 100 mM NaCl, 1 mM EDTA, 1% Triton X-100, 2.5 mM NaF, 2 mM NaPP, 1 mM Na_3VO_4, 1 mM PMSF, 10 μg/mL aprotinin, 1 μg/mL pepstatin, 5 μg/mL leupeptin), and protein amount was determined using the bicinchoninic acid assay (BCA; Thermo Fisher Scientific Inc.). The harvested proteins were then subjected to sodium dodecyl sulphate polyacrylamide (10%) gel electrophoresis (SDS-PAGE) and transferred to a polyvinylidene difluoride (PVDF) membrane (Immobilon-P; Millipore) for Western blot analysis. Immunodetection of each protein was achieved with the primary antibodies (anti-NFAT/c1 and anti-β-actin antibodies) and horseradish peroxidase-conjugated secondary antibodies, followed by SuperSignal Femto chemiluminescence substrate (Thermo Fisher Scientific Inc.).

Determination of glycogen content

Cells were lysed with 50 μL/well of lysis buffer (0.6% perchloric acid and 0.2 M Na-acetate, pH 4.8), sonicated (Sonics Vibra Cell) and kept at -20°C until analysis. After addition of 4 μL of 1 M $KHCO_3$ and 4 μL of 10 mg/mL amyloglucosidase (Roche), cell lysates (40 μL) were incubated at 37°C for 2 hours. The lysates were then centrifuged at 15,000 rpm for 10 minutes and the glucose concentration (derived from glycogen) was determined employing a Determiner GLE (Kyowa Medix, Tokyo Japan) with the positive control being 0.1 mg/mL glycogen (Sigma G-8876, Type III, Rabbit liver). SpectraMax M5 was used with the SoftMAX Pro Windows software program (Molecular Devices, Japan).

Statistical analysis

All data are presented as means and standard errors of the mean (S.E.). Statistical analysis was performed using Student's paired *t*-test. For analysis of the time course of IL-6 production, a one-way ANOVA was applied to determine significant differences between trials. Statistical significance was accepted at $p<0.05$. Each experiment was repeated at least three times.

Results

Effects of EPS-evoked contractile activity on the acquisition of IL-6 production

To investigate the effects of EPS-evoked contraction on the acquisition of IL-6 production in C2C12 myocytes, we applied EPS at 40V/60 mm, 2 ms and 1 Hz to C2C12 undifferentiated myoblasts and differentiated myotubes for 24 h [17, 18]. LG-DMEM containing 5 mM glucose was used and conditioned media with or without 24 h EPS were collected for determining the amount of released IL-6 by ELISA. As we previously reported [17, 18, 21], vigorous contraction in response to EPS was observed in C2C12 myotubes, but not in myoblasts (data not shown). In C2C12 myoblasts, no IL-6 production was observed even after EPS. In contrast, a large amount of IL-6 was secreted from contractile C2C12 myotubes exposed to 24 h of EPS (Fig. 1A), as we previously reported [17]. IL-6 release from myotubes depended on the frequency of EPS, and EPS at 0.1 Hz resulted in less IL-6 production than that at 1 Hz (Fig. 1B). The time course of the experiment revealed that the acquisition of IL-6 production is not acutely induced after short term EPS, but rather requires EPS longer than 12 h despite the fact that C2C12 myotubes started to contract after 1-2 h of EPS, which concomitantly lead to increased secretions of both CXCL1/KC and CXCL5/LIX [18].

To investigate the possibility that CXCL1/KC and CXCL5/LIX, both of which are released in response to EPS-evoked contraction within 1-3 h [18], could mediate and/or influence the acquisition of EPS-induced IL-6 production in this culture system, we examined the effects of SB225002, an antagonist for CXCR2

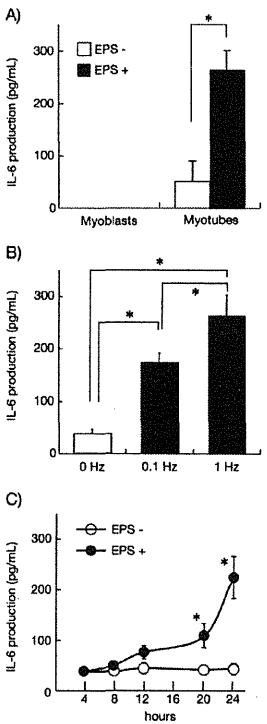

Fig. 1 Characterization of IL-6 production in response to electric pulse stimulation (EPS)-evoked contractile activity

C2C12 myoblasts and C2C12 myotubes were subjected to EPS (40 V/60 mm, 0.1 or 1 Hz frequency, 2-ms duration) for 24 h. DMEM containing 5 mM glucose (LG-DMEM) was used in this experiment. Conditioned medium was collected and subjected to ELISA for measuring IL-6 as described in "*Materials and Methods*." A: comparison of IL-6 production between myoblasts and myotubes B: effect of different frequencies of EPS on IL-6 production in C2C12 myotubes C: time course of EPS-induced IL-6 production from C2C12 myotubes At least 3 independent experiments were performed, and values are means ± SEM (*$p < 0.05$).

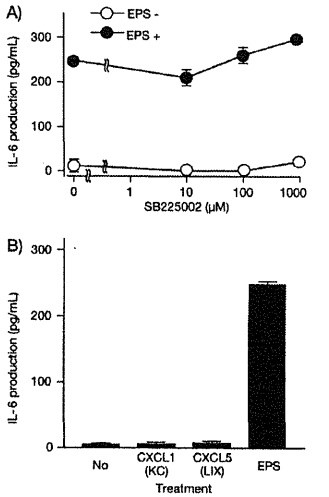

Fig. 2 Effects of contraction-inducible CXC chemokines on EPS-induced IL-6 production

C2C12 myoblasts were treated with EPS (40 V/60 mm, 0.1 or 1 Hz frequency, 2-ms duration) for 24 h in the absence or presence of the indicated factors. DMEM containing 5 mM glucose (LG-DMEM) was used in this experiment and conditioned medium was subjected to ELISA. A: effect of CXCR2 antagonist (SB225002) on EPS-induced IL-6 production in C2C12 myotubes B: effects of CXCL1/KC and CXCL5/LIX on basal IL-6 production during 24 h incubation At least 3 independent experiments were performed, and values are means ± SEM.

serving as a common receptor for both CXCL1/KC and CXCL5/LIX, on EPS-induced IL-6 production (Fig. 2A). Administration of SB225002 during the 24 h of EPS did not influence IL-6 production, indicating that activation of CXCR2 by these CXC chemokines released from contractile C2C12 myotubes was not directly involved in the acquisition of IL-6 production elicited by EPS-evoked contraction. Consistent with this observation, exogenous administration of either CXCL1/KC or CXCL5/LIX failed to induce IL-6 production at least during the 24 h of EPS (Fig. 2B).

Effects of glucose availability and insulin on EPS-induced IL-6 production and cellular glycogen contents along the course of acquisition of contractility

We next examined the effects of extracellular glucose levels on IL-6 production in response to EPS-evoked contraction in C2C12 myotubes. Differentiated C2C12 myotubes were treated with or without 24 h EPS in either LG-DMEM or HG-DMEM, and IL-6 production (Fig. 3A), IL-6 mRNA expression (Fig. 3B) and cellular glycogen content (Fig. 3C) were monitored. After 24 h of EPS-evoked contractile activity, obvious augmentation of IL-6 release and its mRNA expression was observed; however, under HG conditions these increments were significantly blunted. As expected, cellular glycogen contents were significantly higher in C2C12 myotubes cultured under HG conditions than in those cultured under LG conditions (Fig. 3C). Importantly, EPS appeared to be capable of increasing cellular glycogen contents in C2C12 myotubes, and this effect of EPS was obvious when the myotubes were subjected to EPS under HG conditions (Fig. 3C).

We also examined the effects of insulin (100 nM) during 24 h of EPS and found that insulin tended to potentiate EPS-induced IL-6 release and mRNA expression, though the increases did not reach statistical significance. Insulin itself had no stimulatory effect on IL-6 production in terms of either protein or mRNA levels. In addition, we found that insulin-induced glycogen accumulation was markedly enhanced in C2C12 myotubes subjected to 24 h of EPS-evoked contraction. Taken together, these data demonstrate that EPS-induced IL-6 production is markedly affected by glucose availability (Fig. 3A and B), which in closely associated with cellular glycogen contents (Fig. 3C).

Analysis of intracellular signals involved in IL-6 production evoked by EPS-induced contraction

In our previous studies, we demonstrated several intracellular signalling cascades including Erk1/2 and JNK was stimulated by EPS [17, 18]. To characterize the intracellular signals involved in the up-regulation of IL-6 in response to EPS-induced contraction in C2C12 myotubes, we utilized various inhibitors that interfere with specific intracellular signalling cascades. As shown in Fig. 4A, cyclosporine A (CsA), an inhibitor of calcineurin, a calcium-activated phosphatase, completely abolished EPS-induced IL-6 release under

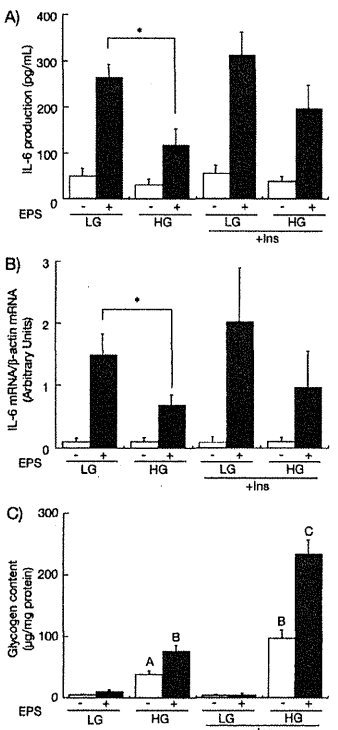

Fig. 3 Effects of extracellular glucose levels on EPS-induced IL-6 production and glycogen accumulation
C2C12 myotubes were subjected to EPS (40 V/60 mm, 1 Hz frequency, 2-ms duration) for 24 h in DMEM containing either 5 mM (LG) or 25 mM (HG) glucose in the absence or presence of 100 nM insulin. A: EPS-induced IL-6 production was measured by ELISA. B: Levels of IL-6 and β-actin (as a control) mRNA expressions were measured by real-time RT-PCR. C: Intracellular glycogen contents were measured after 24 h of culture under each condition. At least 3 independent experiments were performed, and values are presented as means ± SEM ($p < 0.05$, * or different letters denote statistically significant differences).

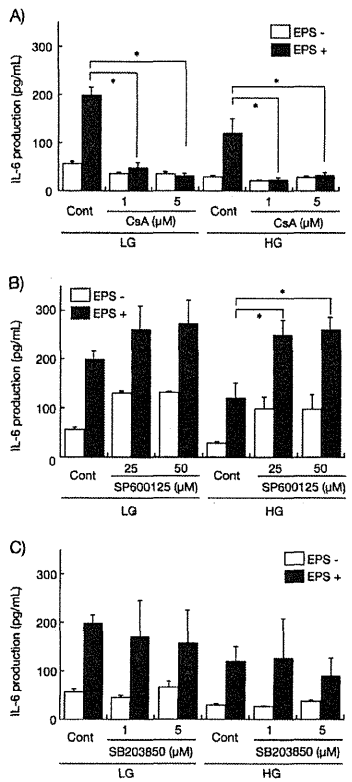

Fig. 4 Effects of cyclosporine A (CsA), SP600125, or SB208350 on EPS-induced IL-6 production
C2C12 myotubes were subjected to EPS (40 V/60 mm, 0.1 or 1 Hz frequency, 2-ms duration) for 24 h in DMEM containing either 5 mM (LG) or 25 mM (HG) glucose. EPS-induced IL-6 production, in the presence of the indicated concentrations of CsA (A), SP600125 (B), or SB203580 (C), was measured by ELISA after 24 h of culture. At least 3 independent experiments were performed, and values are presented as means ± SEM (*$p < 0.05$).

both LG and HG conditions. In contrast, a specific inhibitor for JNK, SP600125, did not blunt, but rather increased, EPS-induced IL-6 production (Fig. 4B). No obvious effect of SB203580, an inhibitor of p38 MAP-kinase, on the EPS-induced IL-6 production was observed (Fig. 4C). It should be noted that CsA, but not other inhibitors, showed slight inhibitory effects on the acquisition of contractile activity induced by EPS (data not shown).

Cellular glycogen contents and EPS-induced IL-6 production in C2C12 myotubes

We further characterized the relationship between cellular glycogen contents and IL-6 expression induced by EPS-evoked contractile activity (Fig. 5). The C2C12 myotubes that underwent pre-exposure to 20 h of EPS under LG conditions, allowing them to become competent in terms of IL-6 production in response to EPS (Fig. 1C), were then supplemented with 1, 5 or 22.5 mM of glucose, and the cells were incubated for an additional 4 h with EPS (Fig. 5A). After 24 h (20 + 4 h) in total of EPS, we measured IL-6 mRNA expression levels (Fig. 5A) and cellular glycogen contents (Fig. 5B) to specifically assess the effects of ambient glucose levels during the last 4 h of EPS. Cellular glycogen levels were very low in C2C12 myotubes after 24 h of EPS under continuous LG conditions (with no additions), but administration of glucose significantly increased cellular glycogen levels during the last 4 h of EPS in a dose-dependent manner (Fig. 5B). Importantly, administration of glucose dose-dependently suppressed the IL-6 mRNA levels elicited by EPS-evoked contraction (Fig 5A). However, administration of pyruvate, a glucose metabolite capable of entering the TCA cycle but which cannot be directly utilized for glycogen synthesis [22], failed to suppress IL-6 mRNA expression (Fig. 5A) with no glycogen accumulation (Fig. 5B).

Although EPS increased dephosphorylation of NFAT/c1 (as assessed by its electrophoretic mobility in SDS-PAGE) (Fig. 5C), a downstream substrate of calcineurin that appears to be involved in the acquisition of EPS-induced IL-6 production (Fig. 3A), administration of either glucose or pyruvate for the last 4 h of EPS did not reverse the EPS-induced mobility shift of NFAT/c1. Note that administration of CsA significantly suppressed the mobility shift of NFAT/c1.

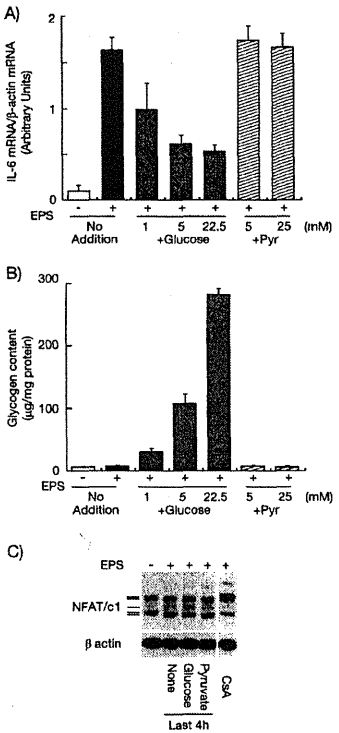

Fig. 5 Effects of glucose supplementation after 20 h of EPS on IL-6 mRNA expression, glycogen accumulation, and NFAT phosphorylation status
C2C12 myotubes were treated with EPS for 20 h in DMEM containing 5 mM glucose (LG) and then the indicated final concentrations of glucose or pyruvate were added to the culture. After an additional 4 h culture with EPS in the absence or presence of nutrient supplementation, levels of IL-6 and β-actin (control) mRNA expression (A) and intracellular glycogen contents (B) were measured. Whole cell lysates were subjected to Western blot analysis using anti-NFAT/c1 and anti-β-actin antibodies (C). At least 3 independent experiments were performed, and values are presented as means ± SEM.

Discussion

Because of highly complex interrelated stimuli evoked by muscle contractile activity, physiological responses of working muscle to physical exercise have mainly been assessed using exercising animal models and human subjects [15, 23]. Recently, we established an advanced *in vitro* muscle contraction model using cultured myotubes displaying vigorous EPS-evoked contractile activity [17, 18, 21]. This model has increasingly been utilized by other researchers for investigating molecular mechanisms underlying various biological responses induced by actual contractile activity of muscle cells [24-27].

In the present study, we observed that acquisition of IL-6 up-regulation in response to EPS-evoked contractile activity was remarkably delayed as compared to the initiation of contraction-inducible CXC chemokines release [18] (Fig. 1), despite the EPS-dependent intracellular Ca^{2+} ($[Ca^{2+}]_i$) transients being immediately elicited, leading to acquisition of obvious contractility within 1 h as well as to increased secretion of these CXC chemokines [17, 21]. Since 30 min of treadmill running was capable of inducing IL-6 expression in working muscles in rodents [5, 17, 26], the contractile C2C12 myotubes apparently require a much longer period of time to acquire the ability to secrete IL-6 in response to contractile activity than do *in vivo* skeletal muscles. Thus, caution must be exercised in interpreting data obtained from an *in vitro* exercise model and it is quite difficult to directly compare the results obtained with *in vivo* data. However, our present study provides several important insights into the regulation of IL-6 expression in response to contractile activity of muscle cells. One of the explanations for the discrepancy between *in vivo* and this *in vitro* model is that the acquisition of IL-6 secreting capability may represent the maturation of regenerating muscle fibers.

Contraction-inducible CXC chemokines and EPS-induced IL-6 regulation

First, it was clearly demonstrated that CXCL1/KC and CXCL5/LIX, both of which began to be secreted from contractile C2C12 myotubes within approximately 1 h of EPS [18], did not influence IL-6 expression in this culture system (Fig. 2A and B). These observations establish that the CXC chemokines do not serve as crucial autocrine factors, at least for this event. It is noteworthy, however, that our previous

report revealed that these contraction-inducible CXC chemokines have autonomous autocrine loops exerting negative feedback on their own secretions [18], and IL-6 reportedly has a positive feedback loop in skeletal muscles [15].

Intracellular signals involved in EPS-induced IL-6 regulation

Second, pharmacological experiments demonstrated that CsA-sensitive calcineurin activity appears to be essential for the acquisition of IL-6 production during 24 h of EPS (Fig. 4A). Given that contraction-inducible CXC chemokines were up-regulated *via* JNK-, but not calcineurin-, mediated signaling cascades [18], expressions of each of these exercise factors appears to be differently regulated at the levels of signaling intermediates upon deciphering the complex contractile activity of muscle cells. In an excellent agreement with our observations, previous reports have indicated involvement of calcineurin activity in exercise-induced IL-6 expression *in vivo* as well as in ionomycin-induced IL-6 expression *in vitro* [23, 28, 29]. On the other hand, several lines of evidence have also indicated the involvement of JNK in exercise-induced up-regulation of IL-6 in working skeletal muscle [30] as well as in the EPS-evoked contracting myotubes [26]. Indeed, various stimuli such as lipopolysaccharides, inflammatory cytokines [31-34], reactive oxygen species [35] and epinephrine [36] have also been shown to increase IL-6 expression in skeletal muscle cells, which are mediated at least in part through the activities of JNK and p38 MAP kinase. In fact, we observed in the present study that inhibition of JNK by SP600125 resulted in a slight increase, rather than a decrease, in IL-6 secretion under both basal and EPS-treated conditions (Fig. 4B). Furthermore, our previous report revealed that the inhibition of p38 MAP kinase by SB-203580 significantly enhanced JNK phosphorylation [18], possibly due to the regulatory loop acting on the JNK-p38 activation system involving a DUSP family of dual-specificity phosphatases [37]. Thus, our present data using pharmacological inhibitors did not allow us to rule out the possibility that JNK and p38 MAP kinase play a role in the regulation of IL-6 expression in response to EPS-evoked contractile activity in concert with the CsA-sensitive signaling cascade, especially under certain nutritional conditions (as discussed in detail in below).

Intracellular glycogen accumulation and EPS-induced IL-6 regulation

Third, a striking observation made in the present study is that administration of glucose to maturated contracting myotubes efficiently dampened the IL-6 mRNA expression in a dose-dependent manner along with intracellular glycogen accumulation, whereas pyruvate completely failed to mimic these glucose actions (Fig. 5). While simple cell culture experiments with 24 h of EPS exposure under HG- and LG-DMEM conditions also indicated possible links among ambient glucose availability, intracellular glycogen contents and EPS-induced IL-6 expression/secretion levels in contractile myotubes (Fig. 3), as shown in previous *in vivo* studies [12, 14], the aforementioned acute nutritional manipulation experiments further support the notion that glycogen accumulation, but not simply energy source supply, is involved in attenuations of contraction-induced IL-6 expression in muscle cells.

Intriguingly, however, delayed administration of glucose failed to reverse the CsA-sensitive EPS-induced mobility shift of NFAT/c1 (Fig. 5C), suggesting that the impacts on IL-6 expression of glucose availability along with intracellular glycogen accumulation are likely mediated through other intracellular signaling pathway(s), rather than the calcineurin-NFAT/c1 signaling cascade, which had a distinct role in the acquisition of contraction induced IL-6 production. In this regard, a previous *in vivo* study demonstrated that low pre-exercise intramuscular glycogen content enhanced IL-6 mRNA expression during 60 min of exercise concomitantly with increased nuclear abundance of phosphorylated p38 MAP kinase in human subjects [30], although direct links among these phenomena were not fully investigated. Thus, a future study will be necessary to clarify details of the possible cross-talk between the stress-responsive MAP kinases and calcineurin signaling cascades under intracellular glycogen titrated conditions by manipulating ambient glucose levels as well as the duration of glucose availability and the timing of administration during culture.

Glycogen accumulation and EPS-evoked contractile activity

Another key observation reported in the present study is the unexpectedly enhanced glycogen accumulations in contracting myotubes during 24 h of EPS under HG conditions (Fig. 3C). It has been well established employing *in vivo* studies that intracellular glyco-

gen contents in working muscles decrease during physical exercise and are eventually depleted by a sufficient amount of exercise [38], even though both enhanced glucose transport mediated *via* GLUT4 translocation [39] and activation of glycogen synthesis occurred simultaneously [40, 41]. Given that EPS-evoked contractile activity significantly increased GLUT4 translocation to the cell surfaces of contracting C2C12 myotubes [17], our present data indicate that glucose uptake is presumably mediated through translocated GLUT4 increased by EPS-evoked contraction, which in turn contributes to the augmented glycogen accumulation. Energy expenditure induced by the EPS-evoked contractile activity burden in the present study (2 ms, 1 Hz, 40 V/60 mm) was perhaps insufficient for consuming all incorporated glucose and, as such, surplus glucose was converted into glycogen under HG conditions (25 mM glucose) even while EPS was persistently applied. On the other hand, as we previously reported, under LG conditions, the extracellular glucose concentration became undetectably low after ~18 h of culture [42], consequently resulting in a marginal intracellular glycogen content regardless of whether insulin was present (Fig. 3C).

Importantly, we also found that insulin stimulation of glycogen accumulation was further augmented in contracting myotubes under the HG condition with EPS. Although glycogen synthase (GS) is well-known to be activated by dephosphorylation *via* inactivation/phosphorylation of GS kinase-3 under insulin treatment, a recent report revealed that an allosteric GS activation by glucose-6-phosphate converted from the incorporated glucose through insulin-mediated GLUT4 translocation is the primary mechanism promoting muscle glycogen accumulation *in vivo* [43]. Thus, increased glycogen accumulations in contracting C2C12 myotubes in the presence of insulin are very likely to reflect increased glucose uptake mediated through GLUT4 translocation induced by both EPS-evoked contractile activity and insulin [17]. In any case, the present data further strengthen our previous reports that the "*in vitro* contraction model" can faithfully display one of the most important aspects of the beneficial effects of exercise, *i.e.* improvement of insulin responsiveness in terms not only of GLUT4 translocation [17] but also of glycogen accumulation.

Since several lines of evidence demonstrated IL-6 to have the ability to increase glucose metabolism as well as insulin actions in skeletal muscles [44, 45], future studies are anticipated to focus on whether the IL-6 released from the contracting myotubes serves as an autocrine factor improving the insulin responsiveness and/or augmented glycogen accumulations observed in EPS-treated cells in this culture system. Finally, given that insulin alone had no impact on IL-6 expression without EPS but tended to potentiate EPS-induced IL-6 up-regulation even under HG conditions with remarkable increases in glycogen accumulation, IL-6 regulation in response to EPS-evoked contractile activity is apparently dependent on various cellular contexts and is subject to highly complex regulatory mechanisms. While interrelations/cross-talks between insulin-and EPS-induced intracellular signaling cascades have yet to be examined, it is highly likely that insulin stimulation alters EPS-induced IL-6 regulation by modulating these intracellular signals in addition to glycogen accumulation. Further studies will be necessary to resolve this important issue.

Acknowledgement

The authors thank Fumie Wagatsuma and Natsumi Emoto for their technical assistance. This study was supported by grants from the Ministry of Education, Science, Sports and Culture of Japan (#22590969 and #20001007) and the JST A-STEP (AS2321552G). This study was also partially supported by Banyu Life Science Foundation International and Takeda Science Foundation.

References

1. Pedersen BK, Febbraio MA (2012) Muscles, exercise and obesity: skeletal muscle as a secretory organ. *Nat Rev Endocrinol* 8: 457-465.
2. Nielsen AR, Pedersen BK (2007) The biological roles of exercise-induced cytokines: IL-6, IL-8, and IL-15. *Appl Physiol Nutr Metab* 32: 833-839.
3. Croisier JL, Camus G, Venneman I, Deby-Dupont G, Juchmes-Ferir A, Lamy M, Crielaard JM, Deby C, Duchateau J (1999) Effects of training on exercise-induced muscle damage and interleukin 6 production. *Muscle Nerve* 22: 208-212.
4. Ostrowski K, Rohde T, Zacho M, Asp S, Pedersen BK (1998) Evidence that interleukin-6 is produced in human skeletal muscle during prolonged running. *J Physiol* 508 : 949-953.
5. Jonsdottir IH, Schjerling P, Ostrowski K, Asp S, Richter EA, Pedersen BK (2000) Muscle contractions induce interleukin-6 mRNA production in rat skeletal muscles. *J Physiol* 528: 157-163.
6. Hiscock N, Chan MH, Bisucci T, Darby IA, Febbraio MA (2004) Skeletal myocytes are a source of interleukin-6 mRNA expression and protein release during contraction: evidence of fiber type specificity. *FASEB J* 18: 992-994.
7. Febbraio MA, Hiscock N, Sacchetti M, Fischer CP, Pedersen BK (2004) Interleukin-6 is a novel factor mediating glucose homeostasis during skeletal muscle contraction. *Diabetes* 53: 1643-1648.
8. Ruderman NB, Keller C, Richard AM, Saha AK, Luo Z, Xiang X, Giralt M, Ritov VB, Menshikova EV, Kelley DE, Hidalgo J, Pedersen BK, Kelly M (2006) Interleukin-6 regulation of AMP-activated protein kinase. Potential role in the systemic response to exercise and prevention of the metabolic syndrome. *Diabetes* 55: S48-54.
9. Pedersen BK, Akerstrom TC, Nielsen AR, Fischer CP (2007) Role of myokines in exercise and metabolism. *J Appl Physiol* 103: 1093-1098.
10. Nehlsen-Cannarella SL, Fagoaga OR, Nieman DC, Henson DA, Butterworth DE, Schmitt RL, Bailey EM, Warren BJ, Utter A, Davis JM (1997) Carbohydrate and the cytokine response to 2.5 h of running. *J Appl Physiol* 82: 1662-1667.
11. Nieman DC, Nehlsen-Cannarella SL, Fagoaga OR, Henson DA, Utter A, Davis JM, Williams F, Butterworth DE (1998) Influence of mode and carbohydrate on the cytokine response to heavy exertion. *Med Sci Sports Exerc* 30: 671-678.
12. Febbraio MA, Steensberg A, Keller C, Starkie RL, Nielsen HB, Krustrup P, Ott P, Secher NH, Pedersen BK (2003) Glucose ingestion attenuates interleukin-6 release from contracting skeletal muscle in humans. *J Physiol* 549: 607-612.
13. Keller C, Steensberg A, Pilegaard H, Osada T, Saltin B, Pedersen BK, Neufer PD (2001) Transcriptional activation of the IL-6 gene in human contracting skeletal muscle: influence of muscle glycogen content. *FASEB J* 15: 2748-2750.
14. Steensberg A, Febbraio MA, Osada T, Schjerling P, van Hall G, Saltin B, Pedersen BK (2001) Interleukin-6 production in contracting human skeletal muscle is influenced by pre-exercise muscle glycogen content. *J Physiol* 537: 633-639.
15. Keller P, Keller C, Carey AL, Jauffred S, Fischer CP, Steensberg A, Pedersen BK (2003) Interleukin-6 production by contracting human skeletal muscle: autocrine regulation by IL-6. *Biochem Biophys Res Commun* 310: 550-554.
16. Weigert C, Dufer M, Simon P, Debre E, Runge H, Brodbeck K, Haring HU, Schleicher ED (2007) Upregulation of IL-6 mRNA by IL-6 in skeletal muscle cells: role of IL-6 mRNA stabilization and Ca2+-dependent mechanisms. *Am J Physiol Cell Physiol* 293: C1139-1147.
17. Nedachi T, Fujita H, Kanzaki M (2008) Contractile C2C12 myotube model for studying exercise-inducible responses in skeletal muscle. *Am J Physiol Endocrinol Metab* 295: E1191-1204.
18. Nedachi T, Hatakeyama H, Kono T, Sato M, Kanzaki M (2009) Characterization of contraction-inducible CXC chemokines and their roles in C2C12 myocytes. *Am J Physiol Endocrinol Metab* 297: E866-878.
19. Yaffe D, Saxel O (1977) Serial passaging and differentiation of myogenic cells isolated from dystrophic mouse muscle. *Nature* 270: 725-727.
20. Nedachi T, Kanzaki M (2006) Regulation of glucose transporters by insulin and extracellular glucose in C2C12 myotubes. *Am J Physiol Endocrinol Metab* 291: E817-828.
21. Fujita H, Nedachi T, Kanzaki M (2007) Accelerated de novo sarcomere assembly by electric pulse stimulation in C2C12 myotubes. *Exp Cell Res* 313: 1853-1865.
22. Kruszynska YT, Ciaraldi TP, Henry RR (2011) Regulation of Glucose Metabolism in Skeletal Muscle. *Compr Physiol 2011, Supplement 21: Handbook of Physiology, The Endocrine System, The Endocrine Pancreas and Regulation of Metabolism* 579-607.
23. Banzet S, Koulmann N, Simler N, Birot O, Sanchez H, Chapot R, Peinnequin A, Bigard X (2005) Fibre-type specificity of interleukin-6 gene transcription during muscle contraction in rat: association with calcineurin activity. *J Physiol* 566: 839-847.
24. Burch N, Arnold AS, Item F, Summermatter S, Brochmann Santana Santos G, Christe M, Boutellier U, Toigo M, Handschin C (2010) Electric pulse stimulation of cultured murine muscle cells reproduces gene expression changes of trained mouse muscle. *PLoS One* 5: e10970.
25. Lambernd S, Taube A, Schober A, Platzbecker B, Gorgens SW, Schlich R, Jeruschke K, Weiss J, Eckardt K, Eckel J (2012) Contractile activity of human skeletal muscle cells prevents insulin resistance by inhibiting pro-inflammatory signalling pathways. *Diabetologia* 55: 1128-1139.
26. Whitham M, Chan MH, Pal M, Matthews VB, Prelovsek O, Lunke S, El-Osta A, Broenneke H, Alber J, Bruning JC, Wunderlich FT, Lancaster GI, Febbraio MA (2012) Contraction-induced IL-6 gene transcription in skeletal muscle is regulated by c-jun terminal kinase/Activator protein -1. *J Biol Chem* 287: 10771-10779.
27. Nikolic N, Skaret Bakke S, Tranheim Kase E, Rudberg I, Flo Halle I, Rustan AC, Thoresen GH, Aas V (2012)

Electrical pulse stimulation of cultured human skeletal muscle cells as an in vitro model of exercise. *PLoS One* 7, e33203.

28. Banzet S, Koulmann N, Sanchez H, Serrurier B, Peinnequin A, Alonso A, Bigard X (2007) Contraction-induced interleukin-6 transcription in rat slow-type muscle is partly dependent on calcineurin activation. *J Cell Physiol* 210: 596-601.
29. Allen DL, Uyenishi JJ, Cleary AS, Mehan RS, Lindsay SF, Reed JM (2010) Calcineurin activates interleukin-6 transcription in mouse skeletal muscle in vivo and in C2C12 myotubes in vitro. *Am J Physiol Regul Integr Comp Physiol* 298: R198-210.
30. Chan MH, McGee SL, Watt MJ, Hargreaves M, Febbraio MA (2004) Altering dietary nutrient intake that reduces glycogen content leads to phosphorylation of nuclear p38 MAP kinase in human skeletal muscle: association with IL-6 gene transcription during contraction. *FASEB J* 18: 1785-1787.
31. Gallucci S, Provenzano C, Mazzarelli P, Scuderi F, Bartoccioni E (1998) Myoblasts produce IL-6 in response to inflammatory stimuli. *Int Immunol* 10: 267-273.
32. Frost RA, Nystrom GJ, Lang CH (2003) Lipopolysaccharide and proinflammatory cytokines stimulate interleukin-6 expression in C2C12 myoblasts: role of the Jun NH2-terminal kinase. *Am J Physiol Regul Integr Comp Physiol* 285: R1153-1164.
33. Frost RA, Nystrom GJ, Lang CH (2006) Multiple Toll-like receptor ligands induce an IL-6 transcriptional response in skeletal myocytes. *Am J Physiol Regul Integr Comp Physiol* 290: R773-784.
34. Luo G, Hershko DD, Robb BW, Wray CJ, Hasselgren PO (2003) IL-1beta stimulates IL-6 production in cultured skeletal muscle cells through activation of MAP kinase signaling pathway and NF-kappa B. *Am J Physiol Regul Integr Comp Physiol* 284: R1249-1254.
35. Kosmidou I, Vassilakopoulos T, Xagorari A, Zakynthinos S, Papapetropoulos A, Roussos C (2002) Production of interleukin-6 by skeletal myotubes: role of reactive oxygen species. *Am J Respir Cell Mol Biol* 26: 587-593.
36. Frost RA, Nystrom GJ, Lang CH (2004) Epinephrine stimulates IL-6 expression in skeletal muscle and C2C12 myoblasts: role of c-Jun NH2-terminal kinase and histone deacetylase activity. *Am J Physiol Endocrinol Metab* 286: E809-817.
37. Owens DM, Keyse SM (2007) Differential regulation of MAP kinase signalling by dual-specificity protein phosphatases. *Oncogene* 26: 3203-3213.
38. Coyle EF, Coggan AR, Hemmert MK, Ivy JL (1986) Muscle glycogen utilization during prolonged strenuous exercise when fed carbohydrate. *J Appl Physiol* 61: 165-172.
39. Goodyear LJ, Hirshman MF, Valyou PM, Horton ES (1992) Glucose transporter number, function, and subcellular distribution in rat skeletal muscle after exercise training. *Diabetes* 41: 1091-1099.
40. Ivy JL, Kuo CH (1998) Regulation of GLUT4 protein and glycogen synthase during muscle glycogen synthesis after exercise. *Acta Physiol Scand* 162: 295-304.
41. Franch J, Aslesen R, Jensen J (1999) Regulation of glycogen synthesis in rat skeletal muscle after glycogen-depleting contractile activity: effects of adrenaline on glycogen synthesis and activation of glycogen synthase and glycogen phosphorylase. *Biochem J* 344: 231-235.
42. Nedachi T, Kadotani A, Ariga M, Katagiri H, Kanzaki M (2008) Ambient Glucose Levels Qualify the Potency of Insulin Myogenic Actions by Regulating SIRT1 and FoxO3a in C2C12 myocytes. *Am J Physiol Endocrinol Metab* 294: E668-678.
43. Bouskila M, Hunter RW, Ibrahim AF, Delattre L, Peggie M, van Diepen JA, Voshol PJ, Jensen J, Sakamoto K (2010) Allosteric regulation of glycogen synthase controls glycogen synthesis in muscle. *Cell Metab* 12: 456-466.
44. Weigert C, Hennige AM, Brodbeck K, Haring HU, Schleicher ED (2005) Interleukin-6 acts as insulin sensitizer on glycogen synthesis in human skeletal muscle cells by phosphorylation of Ser473 of Akt. *Am J Physiol Endocrinol Metab* 289: E251-257.
45. Glund S, Deshmukh A, Long YC, Moller T, Koistinen HA, Caidahl K, Zierath JR, Krook A (2007) Interleukin-6 directly increases glucose metabolism in resting human skeletal muscle. *Diabetes* 56: 1630-1637.

J. Magn. Soc. Jpn., 36, 239-244 (2012)

Position sensing system using magnetic ribbon type marker

O. Mori, S. Yabukami, O. Ishii*, H. Kanetaka**, T. Ozawa, and S. Hashi***

Faculty of Engineering, Tohoku Gakuin University, *1-13-1 Chuo, Tagajo 985-8537, Japan*

*Graduate School of science and technology studies, Yamagata University, *3-4-33 Zyounan, Yonezawa, 992-8510, Japan*

**Graduate School of Biomedical Engineering, Tohoku University, *6-6 Aoba, Aramaki, Aoba-ku, Sendai 980-8579, Japan*

***Research Institute of Electrical Communication, Tohoku University, *2-1-1 Katahira, Aoba-ku, Sendai 980-8577, Japan*

A position sensing system of nasogastric tube using a wireless magnetic ribbon type marker has been developed. A Qualityfactor of the marker is 121 which is 13 times higher than conventional LC resonated marker. Position accuracy within 6.4mm was obtained when the marker inside a commercial nasogastic tube was parallel translation to 100mm. The marker inside the tube was roughly tracked in esophagus and in trachea of human model.

Key words: wireless magnetic ribbon type marker, position sensing, nasogastric tube

磁性リボンを用いた位置検出システム

森 修，藪上 信，石井 修*，金高弘恭**，小澤哲也，戸修一郎***

東北学院大学工学部，多賀城市中央一丁目 13-1 (〒985-8537)

*山形大学大学院理工学研究科，米沢市城南 3 町目 4-33 (〒992-8510)

**東北大学大学院医工学研究科，仙台市青葉区荒巻字青葉 6-6 (〒980-8579)

***東北大学電気通信研究所，仙台市青葉区片平 2 丁目 1-1 (〒980-8577)

1. はじめに

モーションキャプチャは，人間や物体の動きを 3 次元で記録・検出する技術である．検出方法には光学式，機械式，磁気式など古くから様々な手法が開発されてきた．その中で磁気式のモーションキャプチャ [1),2)]は磁界を計測対象とするため，光学的に遮蔽された空間でも適用可能である．しかし従来のものはマーカにバッテリーや引き出し線を必要とし，例えば生体内部等の使用は制約が大きい．筆者らはこれまでの研究で，マーカへの引き出し線を持たず外来ノイズの影響を受けにくい LC 共振型の磁気マーカを用いた位置検出システムを提案し，マーカの位置および方向が検出可能であることを示した [3),4),5)]．

一方医療現場では，病気や怪我で食事を取れない患者や寝たきりの患者などに対し，鼻から咽喉・食道を通して胃に直接栄養剤を送り込む経鼻チューブが多く使用されている．しかし近年経鼻栄養チューブ挿入の際に気管への誤挿入事故や挿入のし過ぎにより胃を傷つける事故が散発している [6)]．従来これらの対策として，X 線によるチューブ挿入の確認や気泡音による確認がなされているが，これらの方法は放射線被曝や信頼性の問題がある．そこで筆者らは，生体挿入用チューブ先端に細長ワイヤレスの LC 共振マーカを添付した一軸励磁による簡易なチューブの位置検出システムを試作し，おおまかに食道および気管への挿入を見分けることに成功した [7)]．しかし，チューブに添付させる制約上，マーカの構造が煩雑で性能指数が低いことが課題となっていた．そこで今回筆者らは、磁性リボンの磁歪振動を利用した磁気タグマーカに着目した．磁性リボンを用いたマーカはコイルとコンデンサを使用する従来のものに比べて構造が単純で安価であり，性能指数が高いため，より精度の高い位置検出が期待できると考えた．一方これまでに，磁気タグの磁歪振動および指向性を用いた位置検出システムが報告されている [8)]．しかしこれは直線移動する車両の 1 次的な位置をおおまかに検出するものであり，本稿の 3 次元位置および 2 方向角 5 自由度の検出には対応していない．

本稿では磁性リボンの磁気マーカを用いて，想定される位置でマーカ添付チューブを 100 mm 移動させて相対位置精度を評価した．次にチューブを人体模型に挿入し，おおまかに食道および気管への挿入を見分けることができたため報告する．

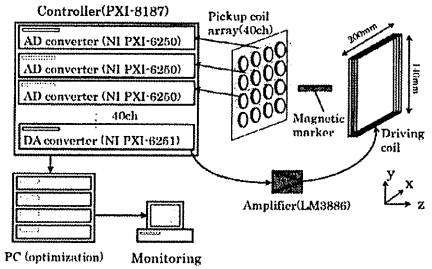

Fig. 1 Schematic diagram of sensing system.

2. 位置計測システムおよび測定方法

Fig. 1 は位置検出システムの構成を示したものである．計測システムはマーカ以外は既報 [7)]と同一の構成であり，励磁コイル，検出コイルアレイ（40 チャンネル），磁性リボンマーカ，生体挿入チューブ，AD および DA コンバータ（NI PXI-6251：1 台），AD コンバータ(NI PXI-6250：10 台），制御ユニット（NI PXI-8187），アンプ（LM3886）から構成される．制御用プログラムは Lab VIEW ver. 7.1，最適化処理プログラムは Visual C++を用いて作成した．本システムではマーカ共振周波数の磁界を印加し，磁性リボンの機械的振動による誘導磁界を検出コイルアレイを用いて計測する．AD コンバータのサンプリングは 250 ksample/sec で測定し，マーカの有無における 40ch の検出コイルの誘起電圧の差分からマーカ寄与電圧を求めた．マーカの中心位置および方向はマーカから発生する誘導磁界がダイポール磁界に近似できることを仮定して，(1)～(3)式より Gauss-Newton 法により最適化処理する．

$$S(\vec{p}) = \sum_{i=1}^{n} \left(B_m^{(i)} - B_c^{(i)}(\vec{p})\right)^2 \tag{1}$$

$$\vec{B}_c^{(i)}(\vec{p}) = \frac{1}{4\pi\mu_0}\left\{-\frac{\vec{M}}{r_i^3} + \frac{3(\vec{M}\cdot\vec{r}_i)\cdot\vec{r}_i}{r_i^5}\right\} \tag{2}$$

$$\vec{p} = (x, y, z, \theta, \phi, M) \tag{3}$$

ただし S は評価値であり，$\vec{p}$ はパラメータベクトルである．i は検出コイルの番号（1～40），$\vec{B}_c^{(i)}(\vec{p})$ は双極子磁界を考慮した磁束密度の理論値，$\vec{r}$ はマーカから検出コイル i への位置ベクトル，$\vec{M}$ はマーカ中心の磁気モーメント，(x,y,z) はマーカ i の座標，θ は xy 平面へ射影したモーメントの方向ベクトルと x 軸のなす角，φ はモーメントの方向ベクトルと z 軸のなす角である．

Fig. 2(a) は今回使用したマーカの写真である．マーカには防犯 IC タグ(高千穂交易社製 DR ラベル)を加工して使用した．このタグには磁性リボン 2 枚と永久磁石が内蔵されている．Fig. 2(b)はマーカ長手方向の断面図で，内部は磁性リボンと永久磁石の 2 重構造になっている．永久磁石は磁性リボンの長手方向にバイアス磁界を印加している．Fig. 2(c)はカッターを用いてマーカを Table 1 のように小型に加工し，生体用チューブ（富士システムズ製 マーゲンゾンデ S，E-10，外径 6mm，内径 4mm）先端に添付したものである．

3. マーカの評価および実験配置

3-1 マーカの共振特性

Fig. 3 に磁性リボンを用いた共振マーカの動作原理について示す．磁性リボンは幅方向に磁気異方性が付与されている．これに励磁コイルから交流磁界を印加すると，磁気モーメントが若干長手方向に傾く．磁性リボンは磁歪により長手方向に機械的に振動し，誘導磁界が発生する．そして

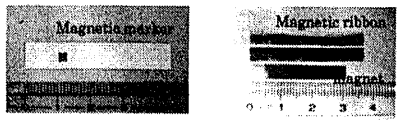

(a) tag

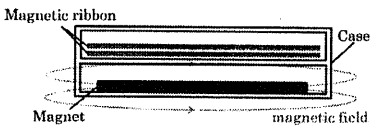

(b) construction of the magnetic ribbon type marker

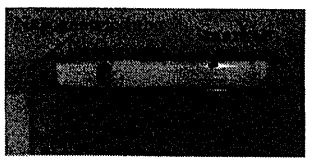

(c) marker in the nasogastric tube

Fig. 2 Magnetic ribbon type marker.

Table 1 Size of magnetic ribbon type marker.

unit:mm

	Before fabrication	Fabricated
Total	45×10×1.9	39×3.8×1.9
Magnetic ribbon	38×5.0×0.03	38×3.6×0.03
Magnet	30×5.0×0.045	30×3.6×0.045

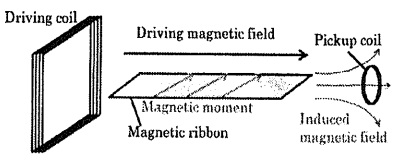

Fig. 3 Principle of operation.

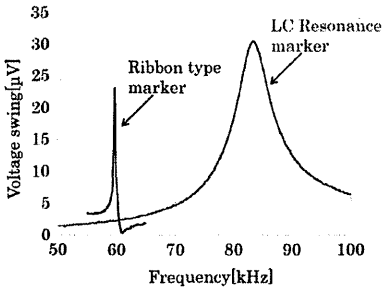

Fig. 4 Comparison of resonance amplitudes.

検出コイルで交流磁界および誘導磁界を測定する．Fig. 4は既報のLC共振マーカ[7]及び磁性リボンマーカの共振周波数における誘導電圧のマーカ寄与分を比較したものである．磁性リボンの機械振動を利用した磁気マーカは，電気的に接続しているLC共振回路に比べて振幅が鋭い．それぞれの共振周波数および性能指数は，LC共振マーカが83.5 kHzで9.03，磁性リボンマーカが59.75 kHzで121.4であり，性能指数は約13.4倍の値となった．LC共振マーカは磁性リボンマーカに比べて検出コイルに近い位置で測定を行っているため信号が強い．なお性能指数Qは(4)式より求めた．

$$Q = \frac{f_r}{\Delta f} \qquad (4)$$

ただしf_rはFig. 4における共振周波数，Δfは共振周波数におけるマーカ寄与電圧の半値幅である．既報[3]で述べたように，本マーカの共振時の性能指数が高いことはマーカの損失が小さく，外部へ発生する誘導磁界が大きいことを意味する．この誘導磁界（等価的な磁気モーメント）はマーカを等価的な共振回路とおくと，マーカの性能指数とマーカの断面積の積に比例する[3]．このことから，高い性能指数を有する機械的振動を利用したマーカにより位置検出システムのSN比が向上すると考えられる．また，本マーカはLC共振型のマーカに比べて周波数選択性が優れているため，共振周波数の異なる複数のマーカの運用に期待できる．

3-2 マーカの指向性

マーカに対してどの角度から磁界を印加すると効率的に誘導磁界が発生し，正確な位置検出が可能であるか検討した．Fig. 5は実験配置及びマーカに印加する磁界の方向を示したものである．検出コイルアレイから300 mmの距離に励磁コイルを対向させるように配置し，その間にマーカを設置した．励磁コイルは140mm×200mmの長方

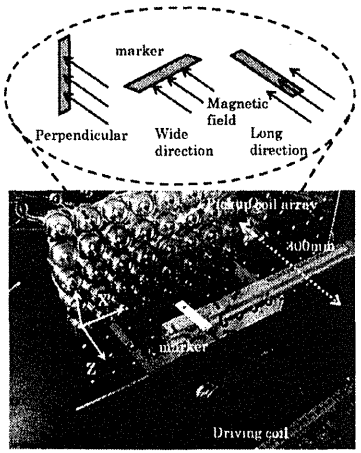

Fig. 5 Examination of directivity.

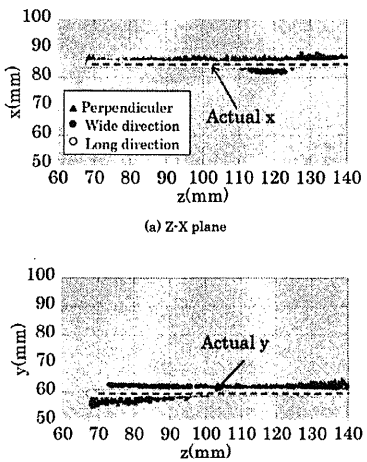

(a) Z-X plane

(b) Z-Y plane

Fig. 6 Position tracking in directivity examination.

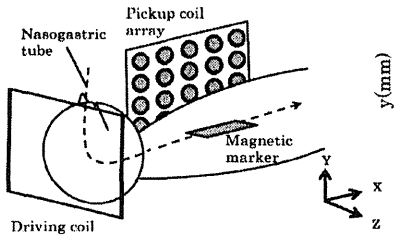

Fig. 7 Experiment arrangement.

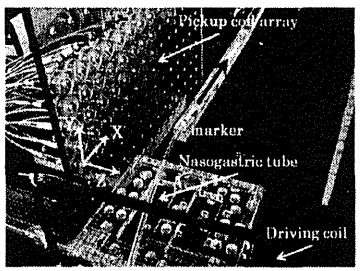

Fig. 8 Position tracking of marker in tube.

形であり，直径1.0mmの銅線を30ターン施した．検出コイルは直径0.2mmの銅線を直径23mm，125ターン施し，同一平面上に30mmの間隔で40個(横:8個×縦:5個)配置した．Fig. 5に示すようにマーカへの印加磁界はそれぞれ面方向，幅方向，長手方向に平行な成分とした．マーカはマイクロメータを用いて，初期値(85,60,70)の位置からz方向に+70 mm直線移動させた．Fig. 6は3通りの位置検出の測定結果であり，(a)はZ-X平面，(b)はZ-Y平面への射影を示している．▲●○はそれぞれ印加磁界を厚み方向，幅方向，長手方向とした場合の最適化されたマーカの中心位置であり，破線は実際の移動の軌跡である．測定結果を見ると，長手方向に磁界を印加した場合が最も実際の軌跡に追従した．一方主としてマーカの幅方向および厚み方向へ励磁した場合，ある程度マーカ位置は最適化できたものの，精度は悪化した．これは主としてマーカの幅方向や厚み方向に磁界を印加した場合，一部の励磁磁界が長手方向成分を持ち，長手方向に機械的振動を起こしたためと考えられる．しかしこの場合は長手方向へ励磁した場合に比較して機械的振動は小さく，誘導磁界が低減したと考えられる．このことから，マーカの長手方向に磁界を印

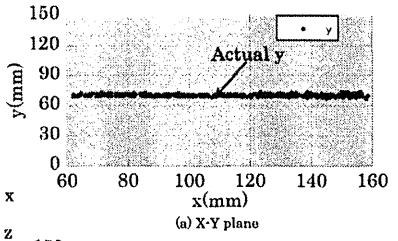

(a) X-Y plane

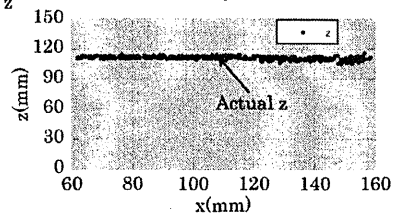

(b) X-Z plane

Fig. 9 Positional detection measurement result.

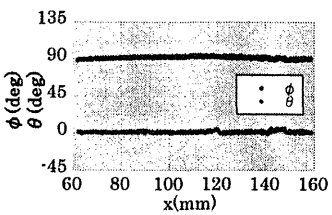

Fig. 10 Direction of marker.

加するのが適切であると考えられる．

3-3 実験配置

Fig. 7は想定している励磁コイル，検出コイルおよび磁気マーカの配置を示したものである．マーカをチューブ内部に貼付する際，チューブは円筒型であるためチューブとマーカの長手方向を平行にする必要がある．また，Fig. 7の指向性の検討より励磁磁界とマーカ長手方向を平行にすることでマーカを効率よく励磁できる．この2つの制約から，励磁コイルを人体の頭上に設置し，励磁方向を人体の長手方向と平行にした．一方，検出コイルはマーカからなるべく強い誘導磁界を得るため，マーカに接近させる必要がある．そのため，人体の胸部付近に設置した．励磁コイルと検出コイルのなす角度は約90°となっている．

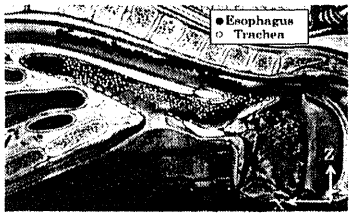

(a) X-Z plane

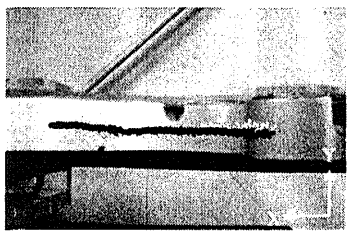

(b) X-Y plane

Fig. 11 Position of the marker in the human model.

4. 実測結果

4-1 直線移動における相対位置精度

食道や気管に相当する位置において，想定する 100mm 程度の移動における相対位置精度およびマーカの向きを評価した．Fig. 8 は励磁コイル，検出コイルの配置およびマーカを移動している写真である．マーカを貼付した生体用チューブ先端をマイクロメータ（SIGMA KOKI 製 LST-16100）およびアクリル棒により検出コイル面から約 110mm の距離 において Fig. 8 の x 方向に+100mm 平行移動した．

Fig. 9 は直線移動時のマーカ中心の軌跡の位置検出結果を示したものである．測定は，マーカを連続的に動かしつつ 10Hz で電圧測定および位置方向を最適化して表示した．(a) は X-Y 平面，(b) は X-Z 平面への射影を示している．●はシステムから得られた測定位置であり，破線は実際の移動の軌跡である．検出された軌跡はほぼ実際の移動距離および軌跡に追従した．100mm 移動での相対位置精度は約 6.4mm 以内であった．Fig. 10 は直線移動時のマーカの向きを φ および θ で検出した結果である．配置したマーカの角度は終始 φ が 90°，θ が 0° であり，実験結果からもこれとほぼ同等の角度が得られた．誤差要因としてはマーカから誘起される磁界とダイポール磁界との誤差，検出コイルのサイズ効果（測定点が広がりをもつことに起因する誤差），AD コンバータのノイズレベル等が考えられる．この値はチューブ先端が食道あるいは気管に入ったことを見分ける観点ではほぼ満足すると考えられる．

4-2 人体模型内部での位置精度

Fig. 11 はマーカを貼付した生体用チューブの先端を人体模型の咽頭付近から気管あるいは食道にそれぞれ挿入し，約 100mm 移動させた場合のマーカの中心位置の軌跡を人体模型の写真と重ねて比較したものである．(a) は X-Z 平面，(b) は X-Y 平面への射影を示している．気管内ストロークの初期配置は (35,70,110)，最終配置は (135,70,105) であり，食道内ストロークの初期配置は (35,70,110)，最終配置は (135,70,125) である．食道・気管共に実際の曲線の軌跡にほぼ追従した結果が得られており，チューブ先端位置が気管にあるか食道にあるかの判別が可能と考えられる．

5. まとめ

1. 磁性リボンの機械的振動を用いた磁気マーカによる位置検出システムを開発した．
2. 試作したマーカは 59.75kHz で性能指数は 121.4 であり，既報 [7] のマーカに対して約 13 倍以上の高い値を得た．
3. チューブ添付マーカを x 軸方向に 100mm 平行移動させた場合、相対位置精度は 6.4mm 以内であった．
4. 先端にマーカを貼付した生体挿入用チューブを人体模型に挿入した場合、チューブ先端位置が気管か食道かの判別が可能である。

謝辞 CPI テクノロジーズの高野卓雄氏，高野卓大氏には本システムの制御プログラムの作成におきまして助力を頂きましたことを深く感謝致します．治具製作にご協力頂いた東北学院大学工学部機械工場スタッフの皆様に感謝致します．本研究の一部は科学技術振興機構研究成果最適展開支援プログラム探索タイプの援助を受けた．

Reference

1) J. E. Mcfee, Y. Das, *IEEE Trans. Antennas ana Propagation*, vol. AP-29, pp. 282-287 (1981).
2) http://www.khk.co.jp/cesd/polhemus.htm
3) S. Yabukami, S. Hashi, Y. Tokunaga, T. Kohno, K. I. Arai, and Y. Okazaki, *Journal of the Magnetics Society of Japan*, vol. 28, pp. 877-885 (2004).
4) S. Yabukami, T. Katoh, S. Hashi, K. I. Arai, and Y. Okazaki, *Journal of the Magnetics Society of Japan*, vol. 30, pp. 218-224, (2006).
5) S. Yabukami, K. Ogasawara, H. Saitoh, S. Hashi, M. Toyoda, Y. Okazaki, and K. I. Arai, *Journal of the Magnetics Society of Japan*, No. 6, pp. 439-444, (2007).
6) http://www.med-safe.jp/pdf/report_6.pdf.
7) R. Sato, S. Yabukami, T. Ozawa, H. Kanetaka, S. Hashi, *Journal of the Magnetics Society of Japan*,35(2), 67-71, (2011).
8) W. Suenaga, *Journal of the Magnetics Society of Japan*, 25, 21 (2001).

2011年11月04日受理，2012年1月18日採録

Chapter 9
Functional Electrical Stimulation (FES) Control for Restoration and Rehabilitation of Motor Function

Takashi Watanabe
Tohoku University, Japan

Naoto Miura
Tohoku University, Japan

ABSTRACT

Functional electrical stimulation (FES) has been studied and clinically applied to restoring or assisting motor functions lost due to spinal cord injury or cerebrovascular disease. Electrical stimulation without control of functional movements is also used for therapy or in rehabilitation training. In recent years, one of the main focuses of FES studies has been its application for rehabilitation of motor function. In this review, the authors first present the basics of applying electrical stimulation to the neuromuscular system for motor control. Then, two methods of FES control are discussed: controllers for FES based on feedback error learning (FEL) and on cycle-to-cycle control of limb movements. The FEL-FES controller can be practical in FES applications that need to control the musculoskeletal system that involves various nonlinear characteristics and delay in its responses to electrical stimulation. The cycle-to-cycle control is expected to be effective in controlling repetitive movements for rehabilitation training. Finally, a study on ankle dorsiflexion control during the swing phase using an integrated system of FES control and motion measurement with wearable sensors for rehabilitation is presented.

INTRODUCTION

Peripheral nerves and muscles can be activated by electrical stimulation. This makes it possible to restore or assist motor functions lost due to spinal cord injury or cerebrovascular disease by applying appropriately regulated current or voltage pulses. This technique is known as Functional Electrical Stimulation (FES) and has been applied to various functions of the motor system, such as upper and lower limb control, respiratory control, assisting urination, and assisting the sensory system through auditory and visual prostheses and sensory substitution.

DOI: 10.4018/978-1-4666-2196-1.ch009

Electrical stimulation that does not control functional movements is also used widely with the aim of producing therapeutic effects; such stimulation is called Therapeutic Electrical Stimulation (TES). TES has been applied clinically for various purposes such as strengthening muscles, reducing spasticity or pain, improving muscle atrophy due to disuse, improving range of motion (ROM), improving volitional movement and urinary incontinence, and preventing bedsores. TES has also been applied for motor rehabilitation.

Application of FES as an orthotic and therapeutic aid in the rehabilitation of upper and lower limb motor function has been one of main focuses of FES studies in recent years. Motor rehabilitation using FES to restore or assist motor function is called FES rehabilitation or FES therapy and has been studied by multiple groups. The therapeutic effects of rehabilitation with FES include improved muscle strength (Merletti et al., 1978; Granz et al., 1996; Yan et al., 2005) and muscle recruitment (Nwesam & Baker, 2004; Yan et al., 2005). Repetitive movement therapy mediated by electrical stimulation also has the potential to facilitate motor relearning (Sheffler & Chae, 2007).

In this review, we first present the basics of applying electrical stimulation to the neuromuscular system in FES applications. Then, two methods of FES control, controllers for FES based on feedback error learning (FEL) and on cycle-to-cycle control of limb movements, are considered in terms of their potential to restore motor functions and movement control during rehabilitation with FES. Finally, an integrated system of FES control and motion measurement using wearable sensors is presented and applied to evaluation of movements in ankle dorsiflexion control.

BASICS OF FES FOR ASSISTING AND RESTORING MOTOR FUNCTIONS

Waveforms of voltage or current stimulation, like those shown in Figure 1, are used in FES applications. When using a monophasic pulse (Figure 1a), the DC component of the pulse is eliminated by a capacitor or transformer to prevent the electrolyzation of stimulation electrodes and damage to the tissue. A charge-balanced biphasic pulse (Figure 1b) can also be used to eliminate the DC component. The biphasic pulse has the advantages that the stimulation effect is larger than that of a monophasic pulse of the same amplitude (A), and the biphasic pulse makes it possible to activate 2 different parts simultaneously in TES (Ogura et al., 2006). Figure 1c shows bursts from several kilohertz to 50 kHz carried by a sine or rectangular wave. Burst wave stimulation is sometimes used to reduce discomfort at the surface

Figure 1. Electrical stimulation waveforms used in assisting and restoring motor function with FES. A: pulse amplitude, T_w: pulse width, $1/T$: pulse frequency

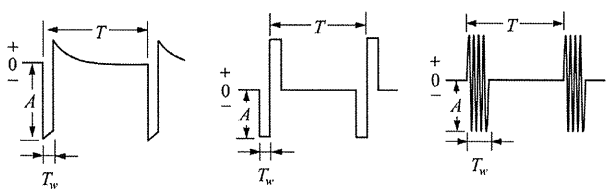

(a) monophasic pulse (b) biphasic pulse (c) high frequency burst wave

electrical stimulation that produces larger muscle contraction force. However, high frequency burst wave stimulation may result in rapid muscle fatigue.

Muscle contraction or muscle force production is controlled by regulating pulse amplitude, pulse width or pulse frequency. Increasing the pulse amplitude and/or the pulse width increases the number of activated motor units (recruitment), which increases muscle contraction force through spatial summation. However, muscle force production based on recruitment by electrical stimulation has nonlinear characteristics including thresholds and saturation. Muscle fatigue also occurs quickly because of the inverse recruitment order in the activation of motor units by electrical stimulation. These are problems for the clinical application of FES because they make control of movements difficult.

Unfused contraction (incomplete tetanus) is caused by low frequency stimulation because each stimulation pulse activates motor units synchronously. On the other hand, tetanic contraction, in which great muscle force is maintained during electrical stimulation, occurs with increases in stimulation frequency. Although further increases in stimulation frequencies produces greater muscle force, muscle fatigue is caused more quickly. For these reasons, pulse frequency modulation is rarely used alone. Usually, muscle contraction is adjusted by amplitude modulation or pulse width modulation with stimulation frequency fixed at about 20 to 30 Hz. When great muscle force must be produced in a short time, as necessary for lower limb movement control, high frequency stimulation at about 40 to 60 Hz is sometimes used.

As shown in Figure 2, there are several methods of applying electrical stimulation to nerves and muscles. Generally, cathodic pulses are applied between two electrodes, when using monophasic pulses. An active electrode is placed near the peripheral nerve or the motor point and a reference electrode is placed over the area that is not affected by electrical stimulation. The surface electrode stimulation method (Figure 2a) uses a pair of electrodes attached to the skin for stimulating one muscle (bipolar configuration), and it is widely used because it is easy to apply. However, it is difficult to selectively stimulate a small muscle or a deep part muscle. Surface stimulation is sometimes accompanied by uncomfortable feelings or pain. The spatial relationship between

Figure 2. Methods of applying electrical stimulation in FES applications. '-' and '+' denote the active electrode and reference electrode, respectively. Broken lines show rough stimulation current flow

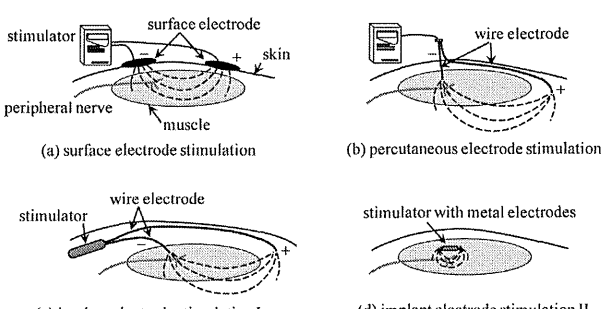

electrode position and motor point may change during muscle contraction, resulting in unstable stimulation effects.

The percutaneous electrode stimulation method shown in Figure 2b uses wire electrodes, and a reference electrode is commonly used for every active electrode (monopolar configuration). The implant electrode stimulation method involves two types of systems: a stimulator and wire electrode system (Figure 2c), and a stimulator with metal electrodes (Figure 2d). The percutaneous and the implant electrode stimulation methods have the same stimulation effect, and they make it practical to restore complex movements by controlling many muscles because it is possible to selectively stimulate a nerve or a muscle by placing an active electrode on the target part.

STUDIES ON FES CONTROL STRATEGY

FES Control Based on Feedback Error Learning

Open-loop control is a major control scheme in current clinical applications of FES. Multichannel open-loop FES control of complicated redundant musculoskeletal systems has become practical clinically since the EMG-based generation method of stimulus pulse amplitude data was established (Handa & Hoshimiya, 1987, Hshimiya et al., 1989; Handa, 1997). However, stimulation data-based open-loop control requires registration of stimulation data for each movement in advance, by which the clinical application of FES is limited to specific movements. Closed-loop control makes it possible to control unregistered movements. In this case, the feedback FES controller has to solve the ill-posed problem of stimulus intensity determination, which arises from the redundancy of the musculoskeletal system. A multichannel feedback controller consisting of multiple proportional-integral-derivative (PID) controllers (Watanabe et al., 2003) could provide a method of solving the ill-posed problem.

The nonlinear characteristics and delays in responses to electrical stimulation limit the effectiveness of feedback FES control of movements. A feedforward controller that has inverse characteristics of the musculoskeletal system can be effective in applying FES to various subjects. Feedback error learning (FEL) (Miyamoto et al., 1998) realizes the inverse model of the controlled limb by training an artificial neural network (ANN) using outputs of a feedback controller. The multichannel PID controller (Watanabe et al., 2003) made it possible to apply the FEL controller to multichannel FES control. The feasibility of the FEL controller for FES (FEL-FES controller) was illustrated with an experimental test of 1-degree-of-freedom (DOF) movement control of the wrist joint with able-bodied subjects (Kurosawa et al., 2005) and a computer simulation test (Watanabe & Fukushima, 2010).

The FEL-FES controller is composed of a multichannel PID controller and a three-layered ANN as shown in Figure 3. The ANN realizes a feedforward controller by learning to acquire a mainly inverse dynamics model (IDM) of the controlled limb using outputs of the feedback controller. The inputs to the ANN are the time series of angles, angular velocities and angular accelerations of target movements at 6 continuous times (Kurosawa et al., 2005). The outputs of the PID controller are described by the following equation:

$$\boldsymbol{I}_{\mathrm{PID}}(n) = \boldsymbol{K}_{\mathrm{P}}\boldsymbol{e}(n) + \boldsymbol{K}_{\mathrm{I}}\sum_{i=0}^{n}\boldsymbol{e}(i) + \boldsymbol{K}_{\mathrm{D}}\{\boldsymbol{e}(n) - \boldsymbol{e}(n-1)\}$$

Here, $\boldsymbol{e}(n)$ is the difference between target and measured joint angles at time n. $\boldsymbol{K}_{\mathrm{P}}$, $\boldsymbol{K}_{\mathrm{I}}$ and $\boldsymbol{K}_{\mathrm{D}}$ are PID parameters, whose values are determined by the expanded Chien-Hrones-Reswick (CHR) method (Watanabe et al., 2003). In calcu-

Figure 3. Block diagram of the FEL controller for FES. θ_T and θ represent the target and the measured joint angles, respectively. The ANN realizes the feedforward controller (inverse dynamics model of the controlled limb) after learning using the outputs of the PID controller while controlling limbs.

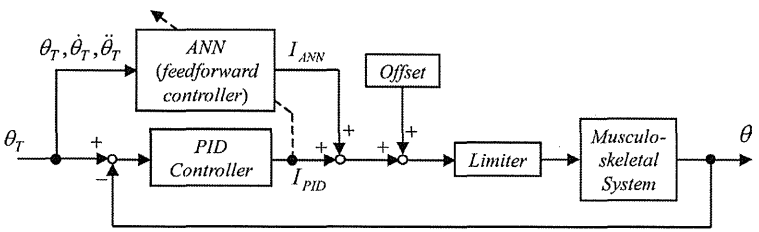

lating the PID parameter values, the ill-posed problem in closed-loop control is solved by using the generalized inverse matrix of the matrix that transforms stimulus intensities into joint angles. Because of the problem of integration windup that is caused by the saturation properties of the musculoskeletal system in response to electrical stimulation, an anti-reset windup (ARW) scheme was applied to the PID controller (Watanabe & Fukushima, 2010). For appropriate ANN training, the integral action of the PID controller is suspended when the total output of the FEL-FES controller (the sum of the outputs of the ANN and the PID controller) saturates.

Learning and control performance were examined in a computer simulation using a musculoskeletal model; the parameters of this model were adjusted to approximate the muscle properties of normal subjects (Watanabe & Fukushima, 2010). Figure 4 shows an example of control results of computer simulation tests, in which tracking controls of 2-DOF movements of the wrist joint (dorsi/palmar and radial/ulnar flexions) were performed stimulating 4 muscles. The stimulated muscles were the extensor carpi radialis longus/bravis (ECRL/B, which are represented by "ECR" because the same stimulation was applied to both), the extensor carpi ulnaris (ECU), the flexor carpi radialis (FCR), and the flexor carpi ulnaris (FCU).

With consideration for clinical applications, target trajectories were generated with the minimum jerk model (Flash & Hogan, 1985) focusing on a two-point reaching movement (Watanabe & Fukushima, 2011). The following cost function was minimized to generate the target trajectories:

$$C_\theta = \frac{1}{2}\int_0^{t_f}\left\{\left(\frac{d^3\theta_1}{dt^3}\right)^2 + \left(\frac{d^3\theta_2}{dt^3}\right)^2\right\}dt$$

where t_f is the movement time. θ_1 and θ_2 are dorsi/palmar and radial/ulnar flexion angles, respectively. The target trajectories were generated on the joint angle plane. First, three target points (A, B and C) were determined randomly. The target was moved from the origin (center) to point C through points A and B, stopping at each point for 1 s. The movement time between two points was 2 s.

As seen in Figure 4, the PID controller successfully solved the ill-posed problem and tracked the target. However, the trajectory on the joint angle plane was different from the target because of delay in the control. The FEL-FES controller improved the delay and tracking performance. The FEL-FES controller made it practical to control

Figure 4 An example of control results with PID or FEL-FES controllers. The ANN was trained with the fixed iteration number of controls (50 trials) using the different target trajectories generated for all control trials. The ANN connection weights were updated after one control trial with the error back-propagation algorithm.

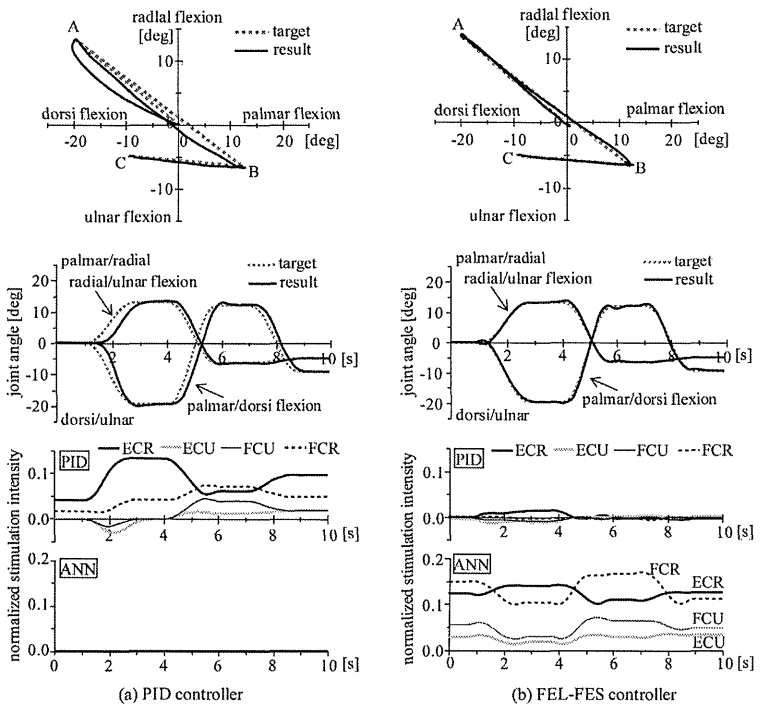

various movements of a musculoskeletal system with nonlinear characteristics and delay.

Although outputs of the feedback controller decreased significantly to small values after ANN learning, their values did not reach zero. This suggests that the ANN did not completely acquire the inverse model. ANN training in 50 control trials using 50 target trajectories obtained the control result shown in Figure 4. Increasing the number of control trials for ANN training and using both inverse static and dynamic models are likely routes to further improve ANN learning.

Cycle-to-Cycle Control of Limb Movements for FES Rehabilitation

In the rehabilitation of motor function, repetitive movement training is often applied to the affected limbs. The repetitive movements of the training can be realized appropriately with closed-loop FES control instead of passive movements by a therapist or open-loop FES control. Closed-loop FES control would be useful for suppressing variations in initial position and muscle response, reducing muscle fatigue during the exercise, and deriving the benefit of electrical stimulation during rehabilitation. Cycle-to-cycle controlled FES aimed at restoring cyclic movements such as gait can be useful for controlling repetitive movements, especially of the lower limbs, in rehabilitation training. This is because trajectory-based closed-loop control of lower limb movements sometimes results in poor tracking and oscillating responses and cannot reach its target due to large inertia and delays in responses.

In order to practically apply cycle-to-cycle control to FES, a fuzzy FES controller was developed to control multi-joint movements (Arifin et al., 2006). The fuzzy control scheme is effective in developing nonlinear controllers, eliminating system identification to determine the controller parameters and simplifying design procedure. The fuzzy FES controller based on the cycle-to-cycle control for clinical applications is shown in Figure 5. Each muscle is stimulated by a single burst of stimulation pulses with a constant pulse amplitude, pulse width and frequency to induce joint movement and reach the target joint angle. The burst duration of stimulation pulses of a current cycle $TB[n]$ is regulated by

$$TB[n] = TB[n-1] + \Delta TB[n]$$

where $TB[n-1]$ is the stimulation burst duration for the cycle just before the current one, and $\Delta TB[n]$ is the output of the fuzzy controller adjusted by the following 2 independent factors: error based output adjustment factors (E-OAF) and sensitivity based OAF (S-OAF) (Watanabe et al., 2009). The E-OAF and the S-OAF are described by fuzzy models in order to adjust the output value based on the error in the previous cycle and based on θ_{ch} / TB in the previous cycle, respectively. θ_{ch} is the joint angle change developed by TB from the angle at the stimulation onset θ_{init}. Therefore, θ_{ch} / TB represents the sensitivity of the muscle. Inputs to the fuzzy controller are the error in the previous cycle and

Figure 5. Block diagram of the cycle-to-cycle control-based fuzzy FES controller with output adjustment factors (E-OAF and S-OAF). θ_T and $\theta_{max}[n]$ represent target and measured maximum angles, respectively. $\theta_{init}[n]$ shows the angle at the stimulation onset. $e[n-1]$ is the error in the cycle just before the current one

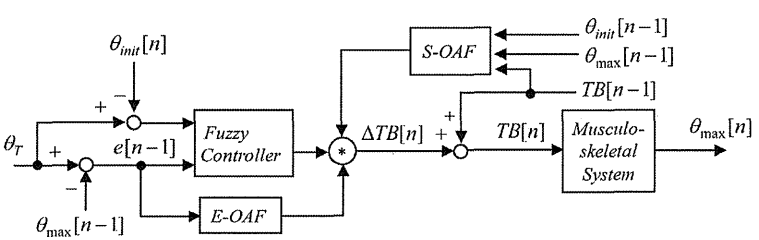

the desired joint angle range for the current control cycle. The desired joint angle range is the required joint angle to reach the target from the angle at the stimulation onset.

Examples of control results of maximum knee joint angles using the wireless surface electrical stimulator are shown in Figure 6. The wireless stimulator was designed and developed using a 2.4 GHz wireless transceiver module for surface stimulation with high voltage monophasic or biphasic pulses (Miura et al., 2011a). The maximum knee flexion angle control was achieved

Figure 6. Examples of control results from the maximum knee extension angle control with a hemiplegic subject and the maximum knee flexion/extension angle control with a neurologically intact subject. Pulse width was 0.3 ms for the hemiplegic subject and 0.2 ms for the neurologically intact subject. Pulse frequency was 20 Hz in both FES controls. In joint angle plots, full knee extension is represented by 0° and positive values indicate knee flexion. Target angles were 65° for the hemiplegic subject in (a) and 50° and 10° for the neurologically intact subject in (b).

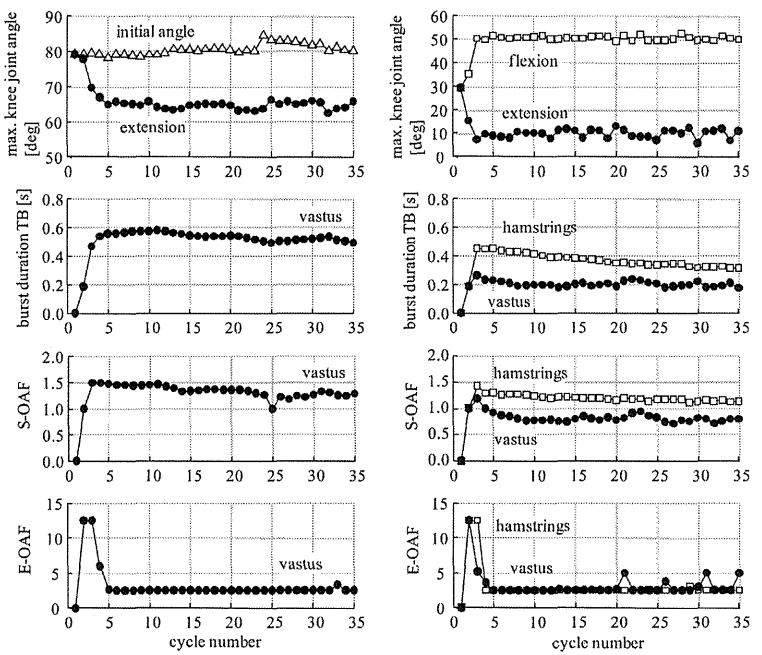

(a) maximum knee extension angle control

(b) maximum knee flexion/extension angle control

by stimulating the vastus muscles of hemiplegic subjects in the sitting position. Maximum knee flexion and extension angle control was achieved by consecutively stimulating the hamstrings and the vastus muscles of neurologically intact subjects sitting on equipment. Knee joint angles measured with an electric goniometer were transmitted to the fuzzy FES controller by wireless communication.

The fuzzy controller based on cycle-to-cycle control developed movements that reached the target within a small number of repeated control cycles. The E-OAF worked effectively in early cycles, nearly reaching the targets within 3 to 5 control cycles. After reaching the target angle, the S-OAF worked to compensate automatically for the different muscle responses between subjects, between control trials or between stimulation cycles. The mean error and variation of developed maximum angles were less than 4° for flexion control and less than 2° for extension control. S-OAF value was large for the hemiplegic subject over most cycles, indicating the S-OAF compensated for the weak muscle response of this subject. For practical applications of the fuzzy controller in rehabilitation training, definitions and detection methods of sensitivity become important (Miura et al., 2011a).

FES SYSTEM FOR REHABILITATION

It is preferable to measure developed movements for objective and quantitative evaluation in rehabilitation training with FES. FES control of a joint may have effects on movements of other joints and/or the contralateral limb (Swigchem et al., 2011). Inertial sensors such as gyroscopes and accelerometers are suitable for this purpose in clinical application because they are small, low cost and easy to set up. Many independent studies have been performed using inertial sensors to detect gait phase (Jasiewicz et al., 2006; Lau & Tong, 2008), measure joint angles or segment inclination angles (Tong & Granat, 1999; Dejnabadi et al., 2005; Findlow et al., 2008; Cooper et al., 2009, Takeda et al., 2009), estimate stride length (Alvarez et al., 2007; Bamberg et al., 2008) and detect stimulus timing for FES (Cikajlo wt al., 2008; Rueterbories et al., 2010). An integrated system of FES control and movement measurement with wearable sensors is expected to be effective in motor rehabilitation.

For motor rehabilitation with FES, surface electrical stimulation is useful because of its non-invasive nature. We developed a prototype system integrating FES control and motion measurement for foot drop correction (Miura et al., 2011b). This system is composed of a wireless surface electrical stimulator, inertial sensors and a PC (Figure 7). The sensors are attached on the lower limbs and the lumber region with stretch bands. The sensor data are transmitted to the PC via a Bluetooth network. Lower limb joint angles and segment inclination angles are calculated from 3-axis components of acceleration and angular velocity measured with the wireless inertial sensors. The inclination angle of each segment is estimated by a Kalman filter and then the joint angles are calculated from the inclination angles (Watanabe et al., 2011; Miura et al., 2011b). The stimulus timing is determined based on the data from the inertial sensor attached on the shank of the paralyzed side. The stimulation data are transmitted to the wireless surface electrical stimulator (Miura et al., 2011a).

Control and measurement using the prototype system was performed on a right hemiplegic subject. The subject was asked to walk 15 m on a level floor at his own speed with or without electrical stimulation. Figure 8 shows an example of the measured joint and inclination angles and the foot strike event. Differences in walking were found in the data from the wearable sensors between the paralyzed and non-paralyzed sides and between with and without FES control. The maximum angles of hip flexion, knee flexion and ankle dorsiflexion of the paralyzed side during the swing phase were smaller than those of the non-paralyzed side. The knee flexion angle of the

Figure 7. A prototype integrated wireless surface stimulator and wireless inertial sensor system for FES control and measurement of lower limb movements

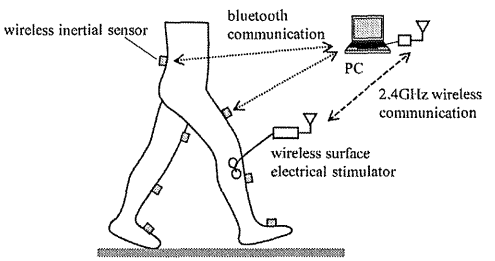

Figure 8. An example of measurement results with or without FES control of ankle dorsiflexion in a hemiplegic subject. Lines below the plots in (c) and (f) show the duration of electrical stimulation applied to the common peroneal nerve. The open square represents the foot strike as detected by the acceleration signals.

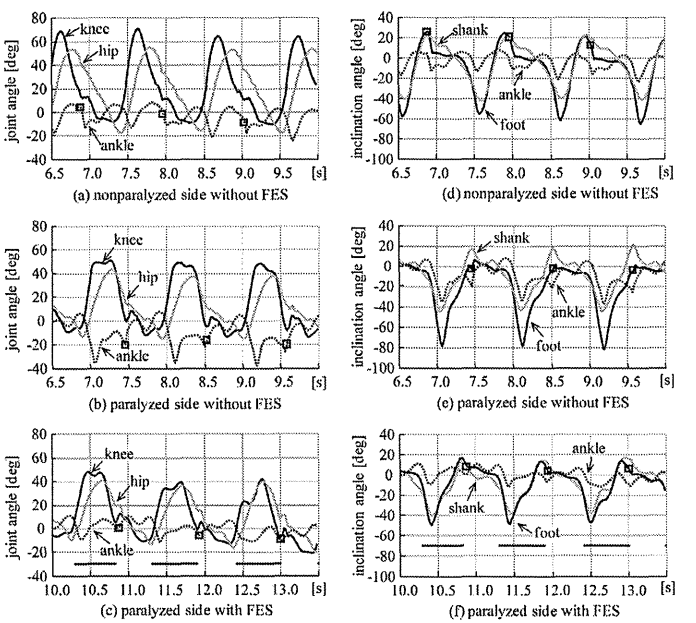

paralyzed side caused two peaks in the swing phase. The foot inclination angle of the paralyzed side at foot strike was about 0° without FES, whereas that of the non-paralyzed side was about 20°. This shows that the foot of the paralyzed side was almost parallel to the ground at the foot strike.

With electrical stimulation to the common peroneal nerve (CPN), the maximum dorsiflexion angle and the foot inclination angle of the paralyzed side increased, and the maximum plantar flexion just after the foot was lifted off the ground decreased. The foot inclination angle just before the foot strike increased to about 20°, the same as that of the non-paralyzed side. This suggests that the foot struck the ground on the heel. Meanwhile, the first peak in knee flexion decreased with electrical stimulation. Stimulation for controlling ankle dorsiflexion also affected knee joint angle.

Taken together, our results indicate that measurement of various angles during FES control can provide useful information for FES rehabilitation. The timings of stimulations were based on the acceleration data from the wearable sensors. The measurement of movement with wearable sensors should also help optimize stimulation triggers for various subjects.

ACKNOWLEDGMENT

The authors thank Dr. Achmad Arifin, Mr. Tomoya Masuko, Mr. Satoru Sugimoto, Mr. Keisuke Fukushima and Mr. Hiroki Saito for their valuable help in the development of the controllers and measurement system, and Dr. Kazunori Seki and Dr. Kiyokazu Akasaka for their support with the clinical examinations.

This study was partly supported by the Ministry of Education, Culture, Sports, Science and Technology of Japan under a Grant-in-Aid for Scientific Research (B), Miyagi Prefectural Government under the Sendai Advanced Preventive Health Care Services Cluster.

REFERENCES

Alvarez, J. C., Gonzalez, R. C., Alvarez, D., Lopez, A. M., & Rodriguez-Uria, J. (2007). Multisensor approach to walking distance estimation with foot inertial sensing. *Proceedings of 29th Annual International Conference of the IEEE Engineering in Medicine and Biology Society*, (pp. 5719-5722).

Arifin, A., Watanabe, T., & Hoshimiya, N. (2006). Design of fuzzy controller of the cycle-to-cycle control for swing phase of hemiplegic gait induced by FES. *IEICE Transactions on Information and Systems. E (Norwalk, Conn.), 89-D*(4), 1525–1533.

Bamberg, S. J., Benbasat, A. Y., Scarborough, D. M., Krebs, D. E., & Para-diso, J. A. (2008). Gait analysis using a shoe-integrated wireless sensor system. *IEEE Transactions on Information Technology in Biomedicine, 12*, 413–423. doi:10.1109/TITB.2007.899493

Cikajlo, I., Matjačić, Z., & Bajd, T. (2008). Efficient FES triggering applying Kalman filter during sensory supported treadmill walking. *Journal of Medical Engineering & Technology, 32*, 133–144. doi:10.1080/03091900601029627

Cooper, G., Sheret, I., McMillian, L., Siliverdis, K., Sha, N., & Hodgins, D. (2009). Inertial sensor-based knee flexion/extension angle estimation. *Journal of Biomechanics, 42*(16), 2678–2685. doi:10.1016/j.jbiomech.2009.08.004

Dejnabadi, H., Jolles, B. M., & Aminian, K. (2005). A new approach to accurate measurement of uniaxial joint angles based on a combination of accelerometers and gyroscopes. *IEEE Transactions on Biomedical Engineering, 52*, 1478–1484. doi:10.1109/TBME.2005.851475

Findlow, A., Goulermas, J. Y., Nester, C., Howard, D., & Kenney, L. P. (2008). Predicting lower limb joint kinematics using wearable motion sensors. *Gait & Posture, 28*(1), 120–126. doi:10.1016/j.gaitpost.2007.11.001

Flash, T., & Hogan, N. (1985). The coordination of arm movements: An experimentally confirmed mathematical model. *The Journal of Neuroscience, 5*(7), 1688–1703.

Granz, M., Klawansky, S., Stason, W., Berkey, C., & Chalmers, T. C. (1996). Functional electrostimulation in poststroke rehabilitation: A meta-analysis of the randomized controlled trials. *Archives of Physical Medicine and Rehabilitation, 77*, 549–553. doi:10.1016/S0003-9993(96)90293-2

Handa, Y. (1997). Current topics in clinical FES in Japan. *Journal of Electromyography and Kinesiology, 7*(4), 269–274. doi:10.1016/S1050-6411(97)00011-4

Handa, Y., & Hoshimiya, N. (1987). Functional electrical stimulation for the control of the upper extremities. *Medical Progress Through Technology, 12*(1-2), 51–63. doi:10.1007/978-94-009-3361-3_6

Hoshimiya, N., Naito, A., Yajima, M., & Handa, Y. (1989). Multichannel FES system for the restoration of motor functions in high spinal cord injury patients: A respiration-controlled system for multijoint upper extremity. *IEEE Transactions on Biomedical Engineering, 36*(7), 754–760. doi:10.1109/10.32108

Jasiewicz, J. M., Allum, J. H., Middleton, J. W., Barriskill, A., Condie, P., Purcell, B., & Li, R. C. (2006). Gait event detection using linear accelerometers or angular velocity transducers in able-bodied and spinal-cord injured individuals. *Gait & Posture, 24*, 502–509. doi:10.1016/j.gaitpost.2005.12.017

Kurosawa, K., Futami, R., Watanabe, T., & Hoshimiya, N. (2005). Joint angle control by FES using a feedback error learning controller. *IEEE Transactions on Neural Systems and Rehabilitation Engineering, 13*(3), 359–371. doi:10.1109/TNSRE.2005.847355

Lau, H., & Tong, K. (2008). The reliability of using accelerometer and gyroscope for gait event identification on persons with dropped foot. *Gait & Posture, 27*, 248–257. doi:10.1016/j.gaitpost.2007.03.018

Merletti, R., Zelaschi, F., Latella, D., Galli, M., Angeli, S., & Bellucci, M. S. (1978). A control study of muscle force recovery in hemiplegic patients during treatment with functional electrical stimulation. *Scandinavian Journal of Rehabilitation Medicine, 10*(3), 147–154.

Miura, N., Watanabe, T., Akasaka, K., & Suzuki, T. (2011b). A clinical trial of a prototype of wireless surface FES rehabilitation system in foot drop correction. *Proceedings of 33rd Annual International Conference of the IEEE Engineering in Medicine and Biology Society*, (pp. 5461-5464), in CD-ROM.

Miura, N., Watanabe, T., Sugimoto, S., Seki, K., & Kanai, H. (2011a). Fuzzy FES controller using cycle-to-cycle control for repetitive movement training in motor rehabilitation: Experimental tests with wireless system. *Journal of Medical Engineering & Technology, 35*(6-7), 314–321. doi:10.3109/03091902.2011.591480

Miyamoto, H., Kawato, M., Setoyama, T., & Suzuki, R. (1988). Feedback-error-learning neural network for trajectory control of a robotic manipulator. *Neural Networks, 1*, 251–265. doi:10.1016/0893-6080(88)90030-5

Nwesam, C. J., & Baker, L. L. (2004). Effect of an electric stimulation facilitation program on quadriceps motor unit recruitment after stroke. *Archives of Physical Medicine and Rehabilitation, 85*, 2040–2045. doi:10.1016/j.apmr.2004.02.029

Ogura, T., Murakami, T., Ozawa, Y., Seki, K., & Handa, Y. (2006). Magnetic resonance imaging of morphological and functional changes of the uterus induced by sacral surface electrical stimulation. *The Tohoku Journal of Experimental Medicine, 208*(1), 65–73. doi:10.1620/tjem.208.65

Rueterbories, J., Spaich, E. G., Larsen, B., & Andersen, O. K. (2010). Methods for gait event detection and analysis in ambulatory systems. *Medical Engineering & Physics, 32*, 545–552. doi:10.1016/j.medengphy.2010.03.007

Sheffler, L. R., & Chae, J. (2007). Neuromuscular electrical stimulation in neurorehabilitation. *Muscle & Nerve, 35*(5), 562–590. doi:10.1002/mus.20758

Swigchem, R., Weerdesteyn, V., Duijnhoven, H. J., Boer, J., Beems, T., & Geurts, A. C. (2011). Near-normal gait pattern with peroneal electrical stimulation as a neuroprosthesis in the chronic phase of stroke: A case report. *Archives of Physical Medicine and Rehabilitation, 92*, 320–324. doi:10.1016/j.apmr.2010.10.038

Takeda, R., Tadano, S., Natorigawa, A., Todoh, M., & Yoshinari, S. (2009). Gait posture estimation using wearable acceleration and gyro sensors. *Journal of Biomechanics, 42*(15), 2486–2494. doi:10.1016/j.jbiomech.2009.07.016

Tong, K., & Granat, M. H. (1999). A practical gait analysis system using gyroscopes. *Medical Engineering & Physics, 21*, 87–94. doi:10.1016/S1350-4533(99)00030-2

Watanabe, T., & Fukushima, K. (2010). An approach to applying feedback error learning for functional electrical stimulation (FES) controller: Computer simulation tests of wrist joint control. *Advances in Artificial Neural Systems, 2010*, 814702. doi:10.1155/2010/814702

Watanabe, T., & Fukushima, K. (2011). A study on feedback error learning controller for FES: Generation of target trajectories by minimum jerk model. *Artificial Organs, 35*(3), 270–274. doi:10.1111/j.1525-1594.2011.01223.x

Watanabe, T., Iibuchi, K., Kurosawa, K., & Hoshimiya, N. (2003). A method of multichannel PID control of 2-degree of freedom of wrist joint movements by functional electrical stimulation. *Systems and Computers in Japan, 34*(5), 25–36. doi:10.1002/scj.10298

Watanabe, T., Masuko, T., & Arifin, A. (2009). Preliminary tests of a practical fuzzy FES controller based on cycle-to-cycle control in the knee flexion and extension Control. *IEICE Transactions on Information and Systems. E (Norwalk, Conn.), 92-D*(7), 1507–1510.

Watanabe, T., Saito, H., Koike, E., & Nitta, K. (2011). A preliminary test of measurement of joint angles and stride length with wireless inertial sensors for wearable gait evaluation system. *Computational Intelligence and Neuroscience, 2011*, 975193. doi:10.1155/2011/975193

Yan, T., Hui-Chan, C. W. Y., & Li, L. S. W. (2005). Functional electrical stimulation improves motor recovery of the lower extremity and walking ability of subjects with first acute stroke: A randomized placebo-controlled trial. *Stroke, 36*(1), 80–85. doi:10.1161/01.STR.0000149623.24906.63

KEY TERMS AND DEFINITIONS

Artificial Neural Network: An artificial neural network (ANN), or neural network (NN), is a mathematical or computational model based on the function and/or structure of biological neural systems. An ANN consists of connected artificial neurons whose connection weights are changed by learning to accomplish a specific function.

Cycle-to-Cycle Control: Cycle-to-cycle control is a control method for restoring cyclic movements, such as gait, using FES. During movement control, each characteristic point (for example, maximum flexion angle) is controlled by applying a single burst of stimulation pulses of constant amplitude, width and frequency. Each electrical stimulation is based on an open-loop control of each cycle of movement, i.e., the stimulation burst duration is adjusted based on the evaluation of the previous cycle of movement.

Feedback Error Learning: Feedback error learning is a learning method for artificial neural networks to implement feedforward control. The output of a feedback controller is used as the error during training. Feedback error learning was originally proposed as a model of motor learning in the cerebellum.

Foot Drop: Foot drop is a symptom characterized by ankle dorsiflexion (moving the toe upward around the ankle joint) inability or difficulty due to weakness or paralysis of the dorsiflexor muscles. Foot drop has various causes including stroke, dorsiflexor injuries, peripheral nerve injuries, and neuropathies.

Functional Electrical Stimulation (FES): Functional electrical stimulation (FES) is a technique for restoring or assisting the motor functions of subjects paralyzed due to spinal cord injury or cerebrovascular disease. Appropriately regulated electrical stimulation current or voltage pulses are externally applied to peripheral nerves or muscles to activate muscles and develop functional movements.

Fuzzy Controller: The fuzzy controller works by utilizing a fuzzy inference system expressed in linguistic relations. A basic fuzzy controller consists of three elements: fuzzification, fuzzy inference and defuzzification. Fuzzification converts crisp values into fuzzy values with membership functions. Fuzzy inference converts fuzzy input values to fuzzy output values and formulates a nonlinear mapping from its input space to its output space using "If-Then" type fuzzy rules. Defuzzification converts the output of the fuzzy inference into crisp values that are given to the controlled system using membership functions. The knowledge base defines rules and membership functions using linguistic variables.

Ill-Posed Problem: An ill-posed problem is a problem that has more than one solution. In feedback FES control of the musculoskeletal system, stimulation data for several muscles are calculated from joint angle errors. Generally, the number of muscles is larger than that of the controlled joint angles in motor control of the redundant musculoskeletal system. In this case, stimulation data for the muscles cannot be determined uniquely.

Inertial Sensor: Inertial sensors refer to accelerometers and gyroscopes. An accelerometer measures acceleration and a gyroscope measures angular velocity.

Kalman Filter: The Kalman filter is a recursive filter that estimates the true values of measured signals from noisy signals. By using a Kalman filter, it is possible to obtain an optimal estimation that minimizes the mean square error of the estimated parameters under given constraint conditions. The Kalman filter is used in sensor fusion and data fusion, as fusion provides better estimation than the estimations obtained from one sensor or one measured datum.

PID Controller: A proportional-integral-derivative (PID) controller is a commonly used feedback controller. The PID controller operates by decreasing the error between a measured variable (controlled variable) and a desired or target variable by adjusting the control inputs (manipulated variable). The manipulated variable is the output of the PID controller and is calculated from the error as the weighted sum of three actions, the proportional, integral and derivative actions.

Redundancy: In this review, redundancy refers to the fact that different stimulation data can result in the same movement. Because any human movement is a result of contractions of several muscles (e.g., antagonistic muscle pairs and/or synergistic muscles), various combinations of contraction forces in those muscles can result in the same movement.

Functional Electrical Stimulation (FES) Control for Restoration and Rehabilitation of Motor Function